1 **Acidification, deoxygenation, nutrient and biomasses decline in a**

2 **warming Mediterranean Sea**

4 Marco Reale[1], Gianpiero Cossarini[1], Paolo Lazzari[1], Tomas Lovato[2], Giorgio Bolzon[1], Simona

5 Masina[2], Cosimo Solidoro[1], Stefano Salon[1]

6   1. National Institute of Oceanography and Applied Geophysics - OGS, Trieste, Italy

7   2. Fondazione Centro euro-Mediterraneo sui Cambiamenti Climatici, CMCC, Ocean Modeling

8   and Data Assimilation Division, Bologna, Italy

10 *Correspondence to:* Marco Reale (mreale@inogs.it) and Stefano Salon (ssalon@inogs.it)

12 **Abstract.** The projected warming, nutrient decline, changes in net primary production, deoxygenation and acidification

13 of the global ocean will dramatically affect marine ecosystems during the 21st century. Here we assess the climate change-

14 related impacts in the marine ecosystems of the Mediterranean Sea in the middle and at the end of the 21st century using

15 high-resolution projections of the physical and biogeochemical state of the basin under the Representative Concentration

16 Pathways (RCPs) 4.5 and 8.5. The analysis shows significant changes in the dissolved nutrient content of the euphotic

17 and intermediate layers of the basin, net primary production, phytoplankton respiration and carbon stock (including

18 phytoplankton, zooplankton, bacterial biomass and particulate organic matter). The projections also show a uniform

19 surface and subsurface reduction in the oxygen concentration driven by the warming of the water column and by the

20 increase in respiration. Moreover, we observe an acidification in the upper water column, linked to the increase in the

21 dissolved inorganic carbon content of the water column due to CO_2 absorption from the atmosphere and the increase in

22 respiration. The projected changes are stronger in the eastern Mediterranean due to the limited influence, in that part of

23 the basin, of the exchanges in the Strait of Gibraltar.

25   **1. Introduction**

27 The Mediterranean Sea (Fig. 1) is a mid-latitude semi-enclosed basin surrounded by the continental areas of Southern

28 Europe, Northern Africa and the Middle East. The basin is characterized by a thermohaline circulation composed of three

29 distinctive cells. The first is an open cell associated with the inflow of the Atlantic Water (AW) at the Gibraltar Strait

30 (which undergoes a progressive increase in salinity due to evaporation becoming Modified Atlantic Water, or MAW) and

31 the formation of Levantine Intermediate Water (LIW) in the Eastern basin (Lascaratos, 1993; Nittis and Lascaratos, 1998).

32 The other two are closed cells associated with deep water formation processes occurring in the Gulf of Lions (located in

33 the Northern Western Mediterranean, Fig.1; Somot et al., 2018 and reference therein) and in the Adriatic Sea (Fig. 1;

34 Mantziafou and Lascaratos 2004, 2008; Schroeder et al., 2012 and references therein).

36 Future climate projections for the Mediterranean region based on different emission scenarios show, at the end of the 21st

37 century, (i) a reduction in precipitation and a general warming of the area (e.g., Giorgi, 2006; Diffenbaugh et al., 2007;

38 Giorgi and Lionello, 2008; Dubois et al., 2012; Lionello et al., 2012; Planton et al., 2012; Gualdi et al., 2013; MedEEC,

39 2020), (ii) a warming of seawater (Somot et al., 2006; Adloff et al., 2015; Soto-Navarro et al., 2020; MedECC, 2020),

40 and (iii) a consistent weakening in the thermohaline circulation and an increase in the stratification index throughout the

41 basin (Somot et al., 2006; Adloff et al., 2015; Soto-Navarro et al., 2020) and an increase in frequency and severity of

42 atmospheric and marine heat waves (Galli et al., 2017; Darmaraki et al., 2019). Conversely, the future evolution of sea

43 surface salinity in the Mediterranean Sea and the sign of its change are still uncertain due to the role played by rivers and

44 Gibraltar Strait exchanges (Adloff et al., 2015; Soto-Navarro et al., 2020; MedECC, 2020).
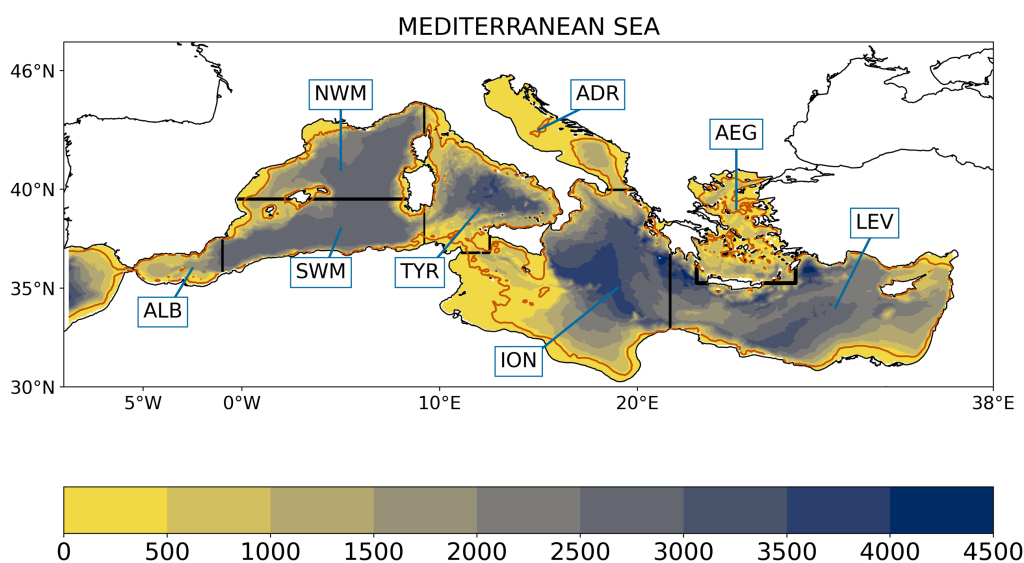
45

46 **Fig.1 Mediterranean Sea bathymetry (in m), the Atlantic buffer zone and relative sub-basins considered in the analysis:**

47 **Alboran Sea (ALB), Southern Western Mediterranean (SWM), Tyrrhenian (TYR), Adriatic Sea (ADR), Ionian Sea (ION),**

48 **Aegean Sea (AEG), Levantine basin (LEV). The dark orange line marks the 200m isobath in the model domain.**

49

50 From a biogeochemical point of view, the Mediterranean Sea is considered as an oligotrophic (ultraoligotrophic in its

51 eastern part) basin (Bethoux et al., 1998; Moutin and Raimbault, 2002; Siokou-Frangou et al., 2010; Lazzari et al., 2012).

52 It is characterized by low productivity levels and an east-west trophic gradient (Crise et al.,1999; D'Ortenzio and Ribera

53 d'Alcala 2009; Lazzari et al., 2012) which results from the superposition of different mechanisms such as the biological

54 pump, the estuarine inverse circulation, and the position of nitrate (NO_3) and phosphate (PO_4) sources (Crise et al., 1999;

55 Crispi et al., 2001). The only exceptions to the oligotrophy of the basin are some areas (Gulf of Lions, Strait of Sicily,

56 Algerian coastlines, Southern Adriatic Sea, Ionian Sea, Aegean Sea and Rhodes Gyre) where strong vertical mixing and

57 upwelling phenomena associated with air-sea interactions and wind stress forcing enrich the surface in nutrients, so

58 favouring phytoplankton rapid growth (or bloom) mostly in the late winter-early spring period (D'Ortenzio and Ribera

59 d'Alcala, 2009). A proxy widely adopted to detect phytoplankton bloom is the surface concentration of chlorophyll-a that

60 is characterized by relative high values in specific open sea/coastal areas, where it is linked to the physical forcing and

61 river inflow (D'Ortenzio and Ribera d'Alcala, 2009; Lazzari et al., 2012; Herrmann et al., 2013; Auger et al., 2014;

62   Richon et al., 2018; Di Biagio et al., 2019; Reale et al., 2020a). The open sea chlorophyll-a vertical dynamics follows a

63   seasonal cycle with winter-early spring surface blooms, and summer onset of a deep chlorophyll maximum (DCM) which

64   deepens from approximately 50 m in the western areas to 100 m in the eastern areas (e.g. Lazzari et al., 2012; Macias et

65   al., 2014; Lavigne et al., 2015).

66

67   Due to the strong links between ocean/atmosphere dynamics and biogeochemical patterns, it has to be expected that future

68   climate change will have relevant impacts on the biogeochemistry and, in turn, on the marine ecosystem dynamics of the

69   Mediterranean Sea. In fact, all the projected physical changes for the region will likely affect vertical mixing and reduce

70   the nutrient supply into the euphotic layer of the Mediterranean Sea (e.g. Richon et al., 2019), which is essential for

71   phytoplankton dynamics and productivity, with possible impacts on the biogeochemical carbon cycle and CO_2 exchange

72   with the atmosphere (e.g., Lazzari et al., 2012; Cossarini et al., 2015; Canu et al., 2015; Solidoro et al., 2021).

73

74   An assessment of the effects of climate change on the biogeochemistry and marine ecosystem dynamics of the

75   Mediterranean Sea has been considered thus far only in a limited number of studies, all focusing on high emission

76   scenarios. Lazzari et al. (2014) found a negative change in the plankton biomass in response to A1B climate change,

77   resulting from an increase of productivity and community respiration. On the other hand, Moullec et al. (2019) under

78   RCP8.5 emission scenario found an increase in both phytoplankton biomass and net primary production by the end of the

79   21st century. Macias et al. (2015) show that, under emission scenarios RCP4.5 and RCP8.5 and despite a significant

80   observed warming trend, the mean integrated primary production rate in the entire basin will remain almost unchanged

81   in the 21st century. However, they pointed out some peculiar spatial differences in the basin such as an increase in the

82   oligotrophy of the western basin due to a surface density decrease and an increase in net primary production in the eastern

83   basin due to the increased density. Richon et al. (2019) observed, under the A2 emission scenario, an accumulation of

84   nitrate in the basin and a reduction of 10% in net primary productivity by 2090, with a peak of 50% in specific areas

85   (including the Aegean Sea). On the other hand, no tendencies in the phosphorus were observed. Pagès et al. (2020)

86   showed, under emission scenario RCP8.5, a decline (stronger in NO_3 than PO_4) in the nutrient concentration at the surface

87   of the basin due to the increase in the vertical stratification and that the Mediterranean Sea will become less productive

88   (14% decrease in integrated primary production in both western and eastern basins) and will be characterized by a

89   reduction (22% in the western basin and 38% in the eastern basin) in large phytoplankton species abundance in favour of

90   small organisms. All these changes will mainly affect the western basin, while the eastern basin will be less impacted

91   (Pagès et al., 2020). Solidoro et al. (2021) discussed the evolution of the carbon cycling, budgets and fluxes of the basin

92   under the A2 scenario, highlighting an increase in the trophodynamic carbon fluxes and showing, at the same time, that

93   the increment in the plankton primary production will be more than compensated by the increase in the ecosystem total

94   respiration, which corresponds to a decrease of the total living carbon and oxygen in the epipelagic layer. Moreover, the

95   work also projected an increase of dissolved inorganic carbon (DIC) pool and quantified for the first time the related

96   acidification of the basin, a process that might significantly alter the Mediterranean ecosystems (Zunino et al., 2017;

97   2019) and their capability to provide ecosystem services (Zunino et al., 2021).

98

99   All of these previous works demonstrate that the dynamics of the marine ecosystem may be affected directly and indirectly

100   by climate change. The warming, acidification and changes in the vertical distribution of the oxygen, nutrient

101   concentration and net primary production related to water column stratification are all potential marine stressors affecting

102   marine organisms and ecosystem dynamics (see Kwiatkowski et al., 2020 for a review about the synergistic effects among

103 potential marine stressors). Moreover, a proper simulation of these marine stressors and related impacts require the
104 adoption of suitable horizontal and vertical resolutions. In fact, it has been shown that meso- and submesoscale structures
105 of the Mediterranean circulation influence indeed the biogeochemical dynamics of many areas of the basin (Richon et al.,
106 2019), while the vertical resolution affects the features of the simulated stratification and subsurface ventilation pathways
107 (see Kwiatkowski et al., 2020 and reference therein for a review).

108

109 These considerations emphasize the importance of providing eddy-resolving future projections of the Mediterranean Sea
110 biogeochemistry that further extend the analysis of the climate change-related impacts in the marine ecosystems of the
111 basin under different emission scenarios. These projections, to the best of the authors' knowledge, have not been analysed
112 so far in the region and that might be used in future studies specifically focused on the analysis of climate change impact
113 on specific organisms, habitats and/or local areas.

114

115 Therefore, here we assess the climate change-related impacts in the marine ecosystems of the Mediterranean Sea in the
116 middle and at the end of the 21st century using eddy-resolving projections (1/16° and 70 vertical levels) of the physical
117 and biogeochemical state of the basin under emission scenarios RCP4.5 and RCP8.5. These projections are derived from
118 the offline coupling between the physical model MFS16 and the transport-reaction model OGSTM-BFM. We focus on
119 21st century projected changes in dissolved nutrients and oxygen, net primary production, respiration, living/nonliving
120 organic matter, plankton and bacterial biomass, and particulate organic matter (POC). Moreover, the response of the basin
121 to the increasing atmospheric CO_2 concentrations is thoroughly investigated. The observed changes are correlated with
122 changes in the physical forcing in the region.

123

124 The article is organized as follows: the MFS16-OGSTM-BFM system along with the physical forcing used to drive the
125 biogeochemical scenarios, initial and boundary conditions and numerical experiments are described in Section 2. Section
126 3 discusses the projected changes in climate change-related impacts in the marine ecosystems of the Mediterranean basin.
127 Finally, Section 4 summarizes and discusses the results of this work, together with their uncertainties, paving the way for
128 possible future research avenues.

129

130 **2. Data and Methods**

131

132 The biogeochemical projections of the Mediterranean Sea state during the 21st century have been produced by driving
133 the transport-reaction model OGSTM-BFM (Lazzari et al., 2012) with the 3D outputs of the physical model MFS16
134 (Oddo et al., 2009) through an off-line coupling. In fact, the physical model MFS16 supplies to the OGSTM-BFM the
135 temporal evolution of daily horizontal and vertical current velocities, vertical eddy diffusivity, potential temperature,
136 salinity, and surface data for solar shortwave irradiance and wind stress. The resulting transport processes affecting the
137 concentration of biogeochemical tracers (advection, vertical diffusion and sinking) are computed by OGSTM, which is a
138 modified version of the OPA tracer model (Foujols et al., 2000). The temporal evolution of biogeochemical processes is
139 computed by the Biogeochemical Flux Model (BFM; Vichi et al., 2015).

140

141

142

143   **2.1. The MFS16 physical model**

144

145   MFS16 is the Mediterranean configuration of the NEMO modelling system (Madec, 2008; see also http://www.nemo-
146   ocean.eu, version 3.4) and constitutes the climate implementation of the Mediterranean Ocean Forecasting System (Oddo
147   et al., 2009; Lovato et al., 2013).

148

149   The model domain covers the whole Mediterranean Sea and part of the neighboring Atlantic Ocean region (Fig.1) with a
150   horizontal grid resolution of 1/16° (~6.5 km) and 72 unevenly spaced vertical levels (ranging from 3 m at the surface
151   down to 600 m in the deeper layers). The model computes the air-sea fluxes of water, momentum and heat using specific
152   bulk formulae tuned for the Mediterranean Sea (Oddo et al., 2009) applied to the atmospheric fields obtained from the
153   atmosphere-ocean general circulation model CMCC-CM (Scoccimarro et al., 2011).

154

155   The open boundary conditions in the Atlantic region for the physical variables (zonal/meridional component of current
156   velocity, sea surface height, temperature and salinity) were derived from the ocean component of the CMCC-CM coupled
157   model, while the riverine freshwater discharges and fluxes in the Dardanelles Strait were provided by the hydrological
158   component of the same coupled model (Gualdi et al., 2013). The initial conditions of the Mediterranean Sea were obtained
159   from the gridded temperature and salinity data produced by the SeaDataNet infrastructure (http://www.seadatanet.org/).
160   The model was initially spun-up for 25 years under present climate conditions and then scenario simulations were
161   performed over the 2005-2100 period.

162

163   **2.2. The OGSTM-BFM transport-reaction model**

164

165   The OGSTM-BFM transport-reaction model is based on the coupling of a transport model (OGSTM) based on the OPA
166   system (Foujols et al., 2000) and the BFM biogeochemical reactor. OGSTM-BFM is fully described in Lazzari et al.
167   (2012, 2016), where it was used to simulate chlorophyll-a, primary production and nutrient dynamics of the Mediterranean
168   Sea for the 1998-2004 period.

169

170   The OGSTM transport model resolves the advection, vertical diffusion and the sinking terms of the biogeochemical
171   tracers. The temporal scheme of OGSTM is an explicit forward temporal scheme for the advection and horizontal
172   diffusion terms, whereas an implicit time scheme is adopted for the vertical diffusion. The BFM biogeochemical reactor
173   considers co-occurring effects of multi-nutrient interactions and energy/material fluxes through the classical food chain
174   and the microbial food web which are both very important in the Mediterranean Sea (Bethoux et al., 1998). BFM has
175   been extensively applied to the studies of the dynamics of dissolved nutrients, chlorophyll-a and net primary production
176   in the Mediterranean Sea (Lazzari et al., 2012; 2016; Di Biagio et al., 2019; Reale et al., 2020a), marine carbon
177   sequestration and alkalinity (Canu et al., 2015; Cossarini et al., 2015; Butenschön et al., 2021), impacts of climate change
178   on the biogeochemical dynamics of marine ecosystems (Lazzari et al., 2014; Lamon et al., 2014; Solidoro et al., 2021),
179   influence of large-scale atmospheric circulation patterns on nutrient dynamics (Reale et al., 2020b) and operational short-
180   term forecasts for the Mediterranean Sea biogeochemistry (Teruzzi et al. 2018; 2019; Salon et al., 2019). The version
181   adopted here is the v5.

182

The model simulates the biogeochemical cycles of carbon, nitrogen, phosphorus and silicon through dissolved forms and living organic and nonliving organic compartments (labile, semi-labile and semi-refractory organic matter). Moreover, it presently includes nine plankton functional types (PFTs), meant to be representative of diatoms, flagellates, picophytoplankton, dinoflagellates, carnivorous and omnivorous mesozooplankton, bacteria, heterotrophic nanoflagellates and microzooplankton. It also simulates the carbonate system dynamics, by solving the set of physical-chemical equilibria related to alkalinity (ALK) and dissolved inorganic carbon (DIC) chemical reaction (Cossarini et al., 2015). Alkalinity variability is driven by processes that alter the ion concentration in seawater (nitrification, denitrification, uptake and release of nitrate, ammonia and phosphate by plankton cells, and precipitation and dissolution of $CaCO_3$, see Wolf-Gladrow et al., 2007). DIC dynamics are driven by biological processes (photosynthesis and respiration, precipitation and dissolution of $CaCO_3$) and physical processes (CO_2 exchanges at the air-sea interface and, as for all the other biogeochemical tracers, dilution-concentration due to evaporation minus precipitation processes).

2.3. Initial and boundary conditions for the biogeochemistry

The initial conditions for the dissolved oxygen, nutrient, silicate and carbonate system variables are based on Medar-Medatlas dataset, as described in Cossarini et al. (2015) and Salon et al. (2019).

Boundary conditions are adopted to represent the external supply of biogeochemical tracers from the Gibraltar Strait and the Mediterranean rivers into the basin. The exchanges of nutrients and other biogeochemical tracers in the Gibraltar Strait are achieved by relaxing the 3D fields in the Atlantic buffer zone (Fig. 1) to average vertical profiles which, for dissolved oxygen, phosphate, nitrate and silicate, refer to Salon et al. (2019) while alkalinity is based on what was described in Cossarini et al. (2015). These profiles do not consider a seasonal cycle or a future temporal evolution, with DIC as the only exception, which is prescribed from a global ocean-climate simulation under RCP8.5 emission scenario performed within the framework of the CMIP5 project (Taylor et al., 2012) and based on the CMCC-CESM modeling system (Vichi et al., 2011). Riverine inputs of phosphate, nitrate, dissolved oxygen, alkalinity and DIC are based on the PERSEUS FP7-287600 project dataset (Van Apeldoorn and Bouwman, 2014) and, also in this case, do not include temporal evolution in the future scenarios.

As observed in previous works (e.g. Richon et al., 2019), a transient scenario for the evolution of the atmospheric deposition of nitrogen and phosphorus over the Mediterranean Sea is presently not available. Following Di Biagio et al. (2019) and Reale et al. (2020a), the atmospheric deposition of phosphate and nitrate is parametrized as a mass flux at the surface and is set for the entire basin equal to 4780 Mmol year^{-1} for phosphate and 81275 Mmol year^{-1} for nitrate. Additional boundary conditions consider the sequestration of inorganic compounds in the marine sediment at the seabed.

Finally, the Representative Common Pathway (RCP) 4.5 and 8.5 emission scenarios (Moss et al., 2010) were used to force the coupled physical-biogeochemical MFS16-OGSTM-BFM system. RCP4.5 represents an intermediate scenario in which CO_2 emissions peak around 2040 (causing the maximum increase in CO_2 concentration), and then decline (with a resulting CO_2 concentration plateau) while the RCP8.5 represents the worst-case scenario, in which CO_2 emissions will continue to increase throughout the 21st century, and the pCO_2 concentration will rise to more than 1200 ppm at the end of the 21st century (IPCC, 2014).

223

2.4. Simulations protocol and set-up

225

226 Long-term simulations can be affected by drifts in state variables due to the imbalance among boundary conditions,
227 transport processes and internal element cycle formulations of the biogeochemical model. Therefore, a specific simulation
228 protocol, based on the use of a control/scenario pairs of simulation, has been implemented in order to disentangle the
229 climate change signal from spurious signals (Solidoro et al., 2021). The protocol consists of a control simulation (CTRL)
230 of 95 years and two 95-year biogeochemical scenario simulations, RCP4.5 and RCP8.5 (Fig.S1 in the supplementary
231 materials), which adopt as initial conditions the resulting final fields from a spin-up simulation. The CTRL repeatedly
232 reproduces an average condition corresponding to the 2005–2014 period looped over the remaining 2015-2100 period for
233 both physical forcing and river discharge (Fig. S1). The difference between each biogeochemical scenario and the CTRL
234 provides the future evolution of a biogeochemical variable due to climate forcing.

235

236 In the simulation protocol we consider, under a specific emission scenario and in the CTRL, the monthly 3D time series
237 of the following variables (X_{bio}): dissolved nutrients and oxygen, chlorophyll-a, net primary production, phytoplankton
238 respiration, organic matter, plankton and bacterial biomass, POC, DIC and pH. The monthly dissolved nutrients and
239 oxygen, organic matter, bacterial biomass, POC, DIC and pH were then vertically averaged over two separate key depth
240 levels: the surface zone and the intermediate zone. The first one spans the upper 100 m of the water column, which
241 represents the location of MAW and the euphotic layer of the basin where most biological activity is concentrated, and
242 where we expect that climate change impacts are the largest. The second one covers the 200-600 m interval, which
243 includes the location of LIW. Only in the case of plankton biomass and chlorophyll-a, the spatial average is limited to the
244 first 100 m of the water column, where the plankton biological activity is mostly concentrated. Finally, for the net primary
245 production and phytoplankton respiration instead of an average, we consider a vertical integral over the first 200 m of the
246 water column (Lazzari et al., 2012).

247

248 From the resulting 2D monthly time series of X_{bio}, we computed the time series of yearly average for the scenario and the
249 CTRL respectively, $X(k)_{SCEN}$ and $X(k)_{CTRL}$ respectively with k = 2005, ..., 2099. As we observed that the model drift
250 present in the CTRL is linear in time, we consider $X_l(k)_{CTRL}$ as the time series built using a linear regression applied to the
251 original $X(k)_{CTRL}$. Then, we defined the time series $X\_evo(k)_{SCEN}$ (with k = 2005, ..., 2099) as:

$$X\_evo(k)_{SCEN} = X_{SCEN} + [X(k)_{SCEN} - X_l(k)_{CTRL}] \quad (1)$$

253 where X_{SCEN} is the average of $X(k)_{SCEN}$ over the 2005-2020 period (hereafter the PRESENT, Fig.S1). $X\_evo(k)_{SCEN}$ is meant
254 to show the temporal evolution (starting from a mean present climate state and filtering from drifts, unbalanced boundary
255 conditions and model errors) of X_{bio} in a specific layer of the water column during the 21st century under a specific
256 emission scenario. The time series of the anomalies of $X\_evo(k)_{SCEN}$ with respect to the PRESENT (hereafter
257 $X\_anom(k)_{SCEN}$) is defined as:

258

$$X\_anom(k)_{SCEN} = X\_evo(k)_{SCEN} - X\_evo_{SCEN-PRESENT} \quad (2)$$

260

261 where $X\_evo_{SCEN-PRESENT}$ is the average of $X\_evo(k)_{SCEN}$ in the PRESENT. Hereafter, if not differently specified, all the shown
262 concentration time series will be represented by $X\_anom(k)_{SCEN}$.

263 To characterize the spatial distribution and the variability of these anomalies within the Mediterranean Sea during the

264 21st century, we consider their horizontally averages in each subbasin defined in Fig. 1, and then in the whole

265 Mediterranean basin scale, in the western Mediterranean (WMED=(ALB+SWM+NWM+TYR)/4) and in the eastern

266 Mediterranean (EMED=(ION+LEV)/2). Moreover, we considered (Fig. S1) two 20-year periods: 2040-2059 (hereafter

267 MID-FUTURE) and 2080-2099 (hereafter FAR-FUTURE), which allow for a robust average computation by removing

268 the effects of the interannual variability. To point out the average anomaly of each variable in each period with respect to

269 the PRESENT we define the metric X_{period}. Being the MID-FUTURE or FAR-FUTURE periods, the average anomalies of

270 the two periods with respect to the PRESENT (in %) are named as $X_{MID-FUTURE}$ and $X_{FAR-FUTURE}$, respectively, and are computed

271 as:

272 $$X_{MID-FUTURE}=100*(evo_{SCEN-MID-FUTURE}-evo_{SCEN-PRESENT})/evo_{SCEN-PRESENT} \quad (3)$$

273 $$X_{FAR-FUTURE}=100*(evo_{SCEN-FAR-FUTURE}- evo_{SCEN-PRESENT})/evo_{SCEN-PRESENT} \quad (4)$$

274 where $evo_{SCEN-MID-FUTURE}$, $evo_{SCEN-FAR-FUTURE}$ and $evo_{SCEN-PRESENT}$ are the averages of $X\_evo(k)_{SCEN}$ for the MID-FUTURE, FAR-FUTURE

275 and PRESENT periods, respectively. Hereafter, if not differently specified, all the concentrations shown in the maps are

276 represented by $X_{MID-FUTURE}$ and $X_{FAR-FUTURE}$.

277

278 **3. Results**

279

280 **3.1 Evaluation of the MFS16-OGSTM-BFM control simulation for the present climate**

281

282 MFS16 modelling system performances under present climate conditions were previously analysed, showing that the

283 main characteristics of the Mediterranean Sea circulation and spatial patterns, mean values and standard deviations of

284 temperature and salinity at different depths in the basin were reliably reproduced (Lovato et al., 2013; Galli et al., 2017).

285 Moreover, the physical reanalysis dataset produced by MFS16 within the Copernicus Marine Environmental Marine

286 Service (CMEMS) (Simoncelli et al., 2019) has already been coupled to the transport-reaction model OGSTM-BFM to

287 carry out a reanalysis for the Mediterranean Sea biogeochemistry (Teruzzi et al., 2019). The latter is a biogeochemical

288 dataset covering the 1999-2015 period at 1/16° resolution, which is already used for validating different biogeochemical

289 simulations in the Mediterranean Sea such as those based on MEDMIT12-BFM (Di Biagio et al., 2019) and RegCM-ES

290 (Reale et al., 2020a) modelling systems. This dataset has been recently upgraded, refining the resolution to 1/24 degree

291 and extending the period to 2019 (Teruzzi et al., 2021).

292

293 To date, no future climate biogeochemical projection of the Mediterranean Sea has been performed through this offline

294 coupling.

295

296 Figure 2 a,b shows the surface average chlorophyll-a (Chl-a) concentrations (upper 10 m) from the CTRL run compared

297 with a climatology based on satellite data available from CMEMS (Colella et al., 2016). The model correctly reproduces

298 the areas in the Mediterranean region characterized by relatively high values of Chl-a: the Alboran Sea, the Gulf of Lions,

299 the coastal areas of the Adriatic Sea, and the Strait of Sicily. Moreover, the CTRL simulation captures the west-east

300 trophic gradient of Chl-a, whose existence has been pointed out in previous works (D'Ortenzio and Ribera d'Alcala,

301 2003; Lazzari et al., 2012; Colella et al., 2016; Richon et al., 2019; Di Biagio et al. 2019; Reale et al., 2020a). On the

302 other hand, we observe a general underestimation of approximately 50% of the Chl-a signal throughout the basin and in

303   the coastal areas probably associated with insufficient river load (Richon et al., 2019; Reale et al., 2020a) and with the
304   tendency of satellite Chl-a measures to be systematically overestimated in the coastal areas with respect to "in situ"
305   observations due to the presence of particulate suspended matter in the water column (Claustre et al., 2002; Morel et
306   Gentili, 2009). Figure 2 also shows the average vertical profiles of Chl-a (c), PO_4 (d), NO_3 (e), dissolved oxygen (f), DIC
307   (g), pH (h) and Alkalinity (i) in the CTRL compared with the recent CMEMS reanalysis (only for Chl-a and pH, Teruzzi
308   et al., 2021) and EMODNET datasets (Buga et al., 2018). The model captures the DCM location, the west-east trophic
309   gradient in the basin, the shape of the vertical profiles, the nutricline depths and low nutrient surface concentrations. Mean
310   simulated values in the first 0-200 m are quite realistic in all the variables. After the spin-up, the simulation reaches a
311   steady state for all the variables in the intermediate/deep layers (not shown). These initial conditions show biases for
312   nutrients and oxygen at a depth of 600 m of approximately 30% lower and 15% higher respectively, than the observations
313   (Fig.2). These biases in the initial conditions come from the spin-up simulation that allows the largest part of the model
314   drifts to be removed. Biases are still present in both the CTRL and scenario simulations while the eventually still-present
315   drifts in the CTRL are by far lower than the climate signal.
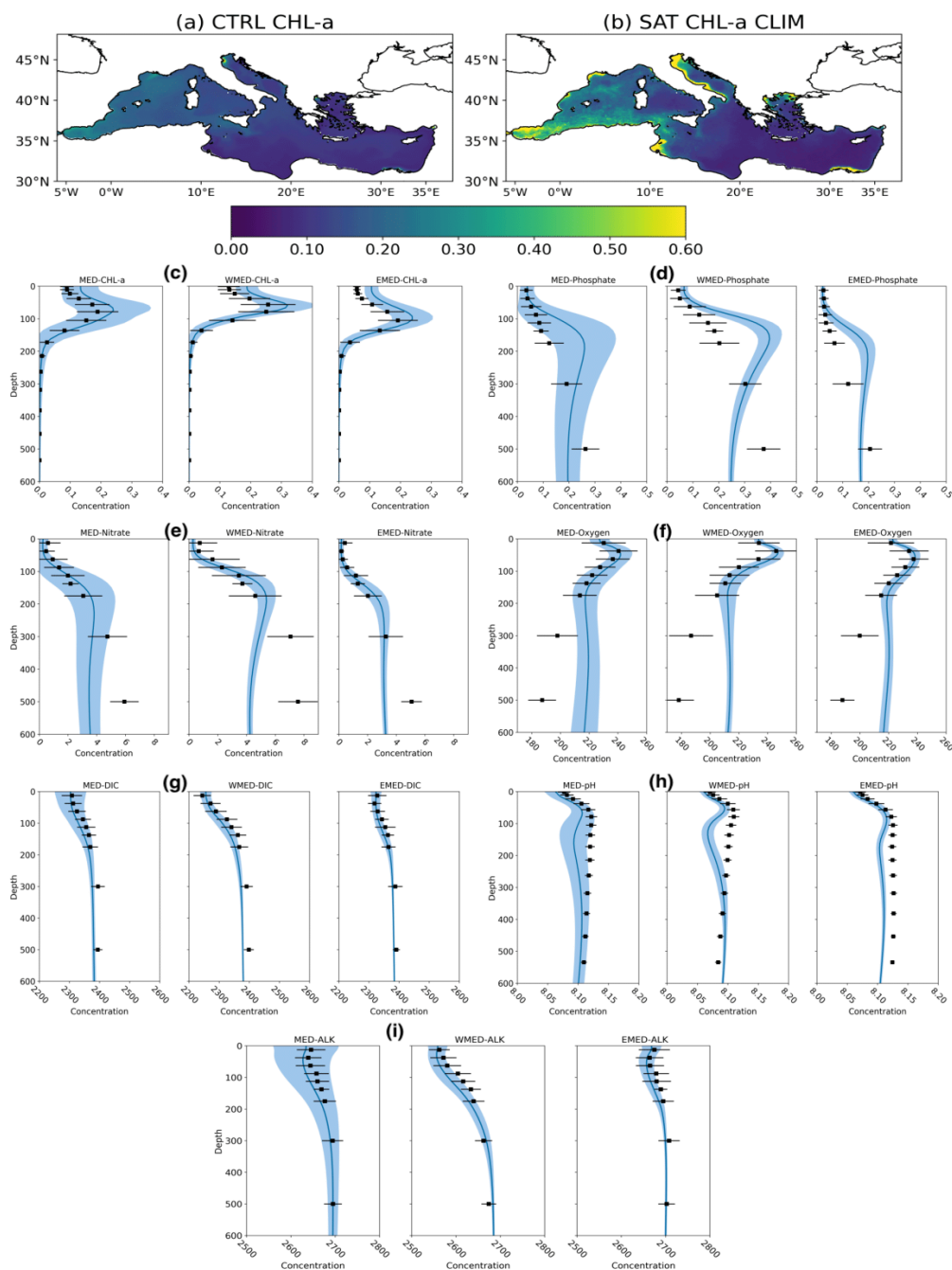
316

317   **Fig.2 Average Chl-a in the first 10m in CTRL (a) for the period 2005-2020 and CMEMS-SAT (b) together with CTRL average**

318   **vertical profiles (blue lines) for the period 2005-2020 of Chl-a (c,mg m⁻³), PO₄ (d, mmol m⁻³), NO₃ (e, mmol m⁻³), Dissolved**

319   **oxygen (f, mmol m⁻³), DIC (g, umol kg⁻¹), pH(h) and Alkalinity (i, umol kg⁻¹). The light blue areas represent the spatial standard**

320   deviation of the monthly modelled data. The modelled data are compared with CMEMS reanalysis (Chl-a and pH) and
321   observations provided by EMODnet (PO₄, NO₃, Dissolved oxygen, DIC, Alkalinity): annual mean (black squares) and related
322   standard deviations (black bars).

323

324   **3.2 Evolution of the thermohaline properties and circulation of the Mediterranean Sea in the 21st century**

325

326   Mean temperature and salinity evolution between 0-100 m and 200-600 m in the 2005-2099 period under the RCP4.5 and
327   RCP8.5 scenarios in the whole Mediterranean Sea and in the western and eastern basins, are shown in Fig. 3. A warming
328   of the surface and intermediate layers is observed at the basin scale and in both the western and eastern basins, whose
329   magnitude (approximately 3°C in the RCP8.5 scenario), agrees with what has already been observed in recent modelling
330   studies based on single/multimodel ensembles (e.g., Adloff et al., 2015; Soto-Navarro et al., 2020).

331

332   On the other hand, the salinity in the surface layer at basin scale and in the eastern basin is characterized by a decrease
333   between 2020 and 2050 followed by a constant increase (stronger in the RCP8.5 scenario) until the end of the 21st century.
334   An increase in salinity also occurs in the intermediate layer both at the basin scale and in the two main subbasins.
335   Conversely, after 2050, the western basin shows a freshening of the surface layer with respect to the beginning of the
336   century, in agreement with what was already observed by Soto-Navarro et al. (2020). Similar to the seawater temperature,
337   the variation in salinity is strongly dependent on the emission scenario with more intense anomalies, both negative and
338   positive, under RCP8.5 conditions (as observed in previous modelling studies as Soto-Navarro et al., 2020).

339

340

341
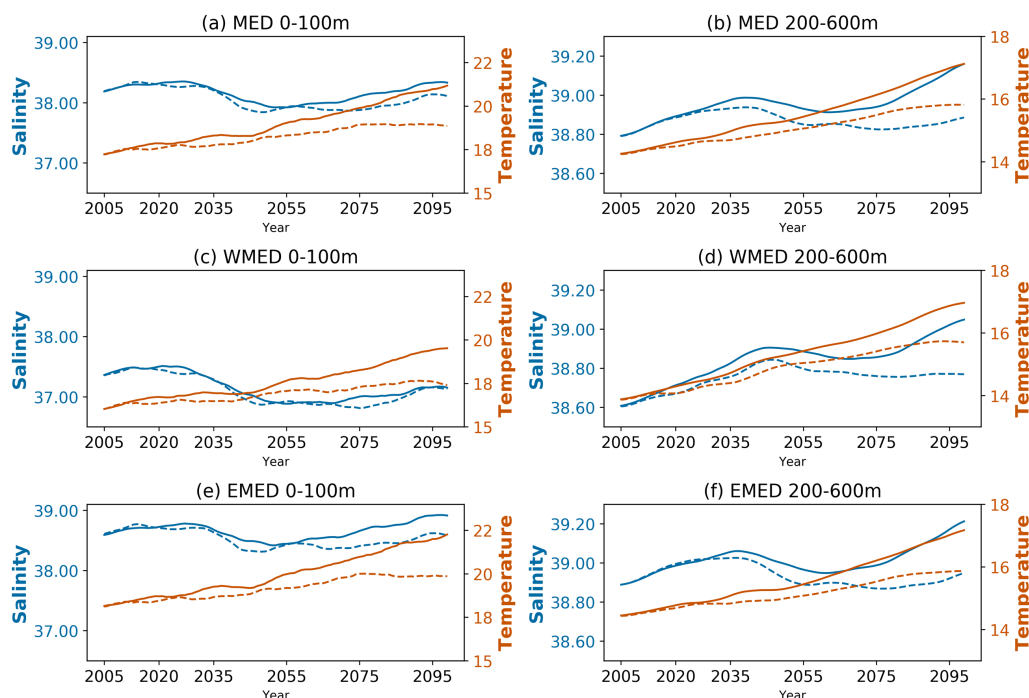
Fig.3 - Yearly timeseries for the period 2005-2099 of Salinity (blue) and Temperature (dark orange, in C) under the emission scenarios RCP8.5 (solid line) and RCP4.5 (dashed line) in the Mediterranean Sea (MED, a-b), Western Mediterranean (WMED, c-d) and Eastern Mediterranean (EMED, e-f) for the layers 0-100 m (left column) and 200-600 m (right column). The yearly timeseries have been smoothed using 10-years running mean.

The spatial distribution of temperature and salinity variations in the surface layer (Fig. S2 in the supplementary materials) shows a comparable basin-scale warming in RCP4.5 and RCP8.5 in the MID-FUTURE (the difference is less than 2%) and a doubled FAR-FUTURE variation in RCP8.5 (17-20%) with respect to RCP4.5 (8-12%), with the north western Mediterranean, Tyrrhenian, Adriatic, Ionian, Aegean Sea and Levantine being the most affected subbasins. Similar relative variations are observed in the intermediate layer (Fig. S2).

General freshening/saltening of the upper/intermediate layers is observed over the entire basin during the MID-FUTURE period (Fig. S3 in the supplementary materials). In the FAR-FUTURE the freshening of the surface is still present at the basin scale in the RCP4.5 scenario (although it is reduced with respect to the MID-FUTURE) and in the western basin in the RCP8.5 scenario. Moreover, an increase in salinity is observed in the Adriatic Sea (in both scenarios) and in the eastern basin under RCP8.5. The decrease in salinity in the 21st century in the western basin is driven by the salinity values imposed in the Atlantic buffer zone (Lovato et al., 2013), while the saltening of the eastern basin is linked to the increased freshwater deficit in the area (e.g., Gualdi et al., 2013; Soto-Navarro et al., 2020). In the intermediate layer, the situation is reversed: while in RCP8.5, the entire basin experiences an increase in the salinity associated with the increase in salinity in the surface water of the eastern basin, in RCP4.5, the eastern basin experiences a slight decrease in salinity associated again with the freshening of surface water. In fact, at the surface, both signals are transported by vertical mixing to the intermediate layers of the eastern basin influencing the salinity of the newly formed LIW.

365   Figure 4 shows the temporal evolution of the Mediterranean thermohaline circulation during the 21st century using the
366   zonal overturning stream function (Myers and Haines, 2002; Somot et al., 2006). The thermohaline circulation of the
367   basin in the PRESENT is composed of two cells, similar to the outcomes of the historical reference experiments described
368   in Adloff et al. (2015) and Waldman et al. (2018). The first cell extends from the surface to 800 m, with a clockwise
369   circulation associated with MAW moving eastwards and LIW moving westwards. The second cell is located between 500
370   and 2500 m in the eastern Mediterranean with a counterclockwise circulation associated with the Eastern Mediterranean
371   Deep Water (EMDW) moving eastwards and LIW moving westwards.

372

373   Under the two scenarios, during the MID-FUTURE period there is an evident weakening of both cells and a reduction of
374   the thickness of the upper layer cell and the eastern basin cell (less than -0.1 Sv), which splits into two sub-cells. By the
375   end of the century both cells show a similar behaviour, whereas in the RCP4.5 scenario, the eastern cell is slightly more
376   intense. The weakening of the zonal overturning stream function is similar to previous findings of Somot et al. (2006)
377   and Adloff et al. (2015). As the Mediterranean thermohaline circulation is driven by both deep and intermediate water
378   formation processes, the overall weakening of both cells is a direct consequence of the increase in the vertical stratification
379   of the water column. In fact, the evolution of the winter maximum mixed layer depth in key convective areas of the
380   Mediterranean Sea, such as the Gulf of Lions, Southern Adriatic, Aegean Sea and Levantine basin (Fig. S4 in the
381   supplementary materials), shows a progressive decrease in the intensity of the open ocean convection after 2030. Only
382   for the Aegean Sea, are the changes in the winter mixed layer maximum depth less marked, with the occurrence of some
383   maxima around 2080 (in RCP8.5) or after 2090 (in RCP4.5), which could correspond to a future tendency of the
384   thermohaline circulation of the Eastern basin to produce EMT-like events (Adloff et al., 2015).

385

386   The projected overall weakening of the Mediterranean thermohaline circulation leads to a reduction in the exchanges of
387   biogeochemical properties between the western and eastern basins through the Sicily strait at both the surface and
388   intermediate levels (Fig.S5 in the supplementary materials) and to a reduced ventilation of intermediate/deep waters
389   (Adloff et al., 2015).

390

391
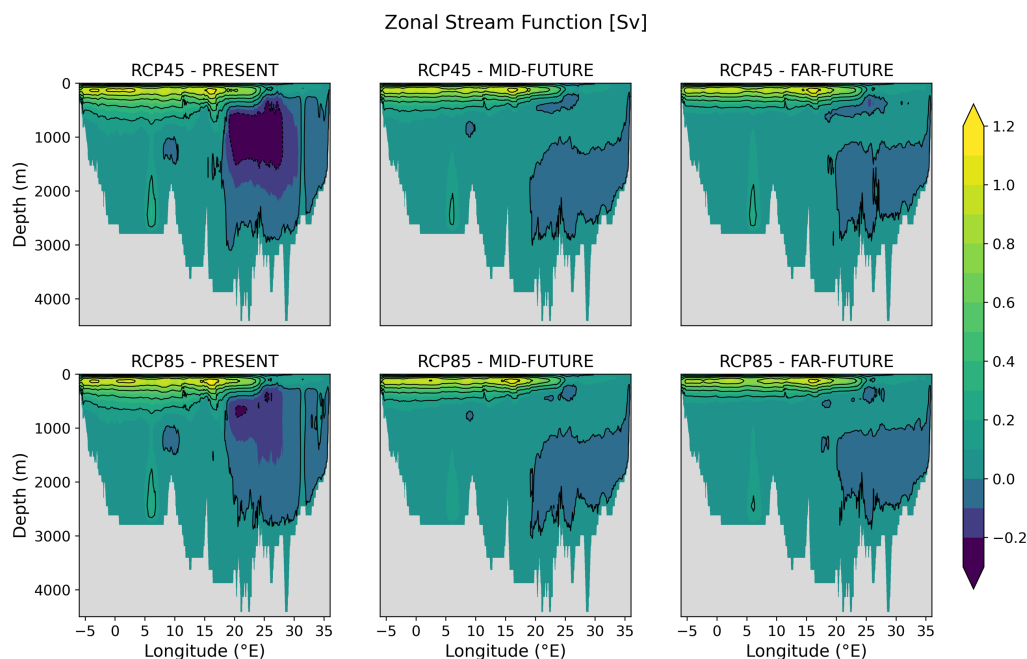
Fig. 4 - Mediterranean Sea zonal stream function annual mean (in Sv) averaged over the PRESENT (2005-2020), MID-FUTURE (2040-2059) and FAR-FUTURE (2080-2099) periods under RCP4.5 and RCP8.5 scenarios.

394

395   **3.3 Spatial and temporal evolution of nutrients, dissolved oxygen and chl-a concentrations**

396

397   Figures 5 and 6 show the spatial distribution of the magnitude and signs of the changes that will affect the dissolved

398   nutrient concentrations during the 21st century. In the FAR-FUTURE, the decreases in PO_4 and NO_3 concentrations in the

399   0-100 m layer under the RCP8.5 scenario are almost double (approximately 13% and 20% for PO_4 and NO_3, respectively)

400   with respect to those observed in the RCP4.5 (approximately 7% and 13%) and are particularly marked in the Levantine

401   basin, in the Aegean Sea and in the Tyrrhenian Sea. On the other hand, an overall increase (stronger in NO_3 than PO_4) is

402   observed in the Northern Adriatic Sea and in many other coastal areas influenced by river dynamics. This signal can be

403   explained by the increase in vertical stratification and the decrease in river discharges (Gualdi et al., 2013) which results

404   in a higher concentration of the nutrients at the river mouths. The increase in the Northern Adriatic is counterbalanced by

405   a decrease in the Southern Adriatic associated with the reduced vertical mixing in the water column and reduced inflow

406   of nutrients through the Otranto Strait (Fig. S6 in the supplementary materials). Moreover, the two scenarios show some

407   significant changes in the dissolved nutrient concentrations at local scale (brown patches) in the Alboran Sea and in the

408   southern Ionian associated with changes in the intensity of mesoscale circulation (eddies) of both areas and in the intensity

409   and spatial structure of the mid-Ionian jet (not shown).

410

411   In contrast to the general decreasing nutrient content of the upper layer, the intermediate layer in both scenarios shows a

412   strong (milder) increase in nutrient concentration in the southern Aegean Sea (Levantine basin, northwestern

413   Mediterranean and Alboran Sea) in the 21st century driven by the reduced vertical mixing, which tends to increase the

414   nutrient content of the intermediate layers. The Tyrrhenian, Ionian and Southern Adriatic Seas are, in turn, characterized

415   by a permanent negative anomaly. In the first two areas, the anomaly can be associated with the decrease in the westward

416   transport of nutrients in the intermediate layers through the Sicily Strait (consequences of the weakening of the zonal

417   stream function discussed in Section 3.2, Fig. S5), while in the Adriatic Sea, the observed changes are driven by the

418   increase in the nutrient export in the intermediate layer through the Otranto Strait (Fig.S6). In the northwestern

419   Mediterranean the observed positive anomalies become weaker and even negative in the FAR-FUTURE under the

420   RCP4.5 emission scenario, likely due to some convective events that take place between 2080 and 2100, as shown in Fig.

421   S4.

422

423

424
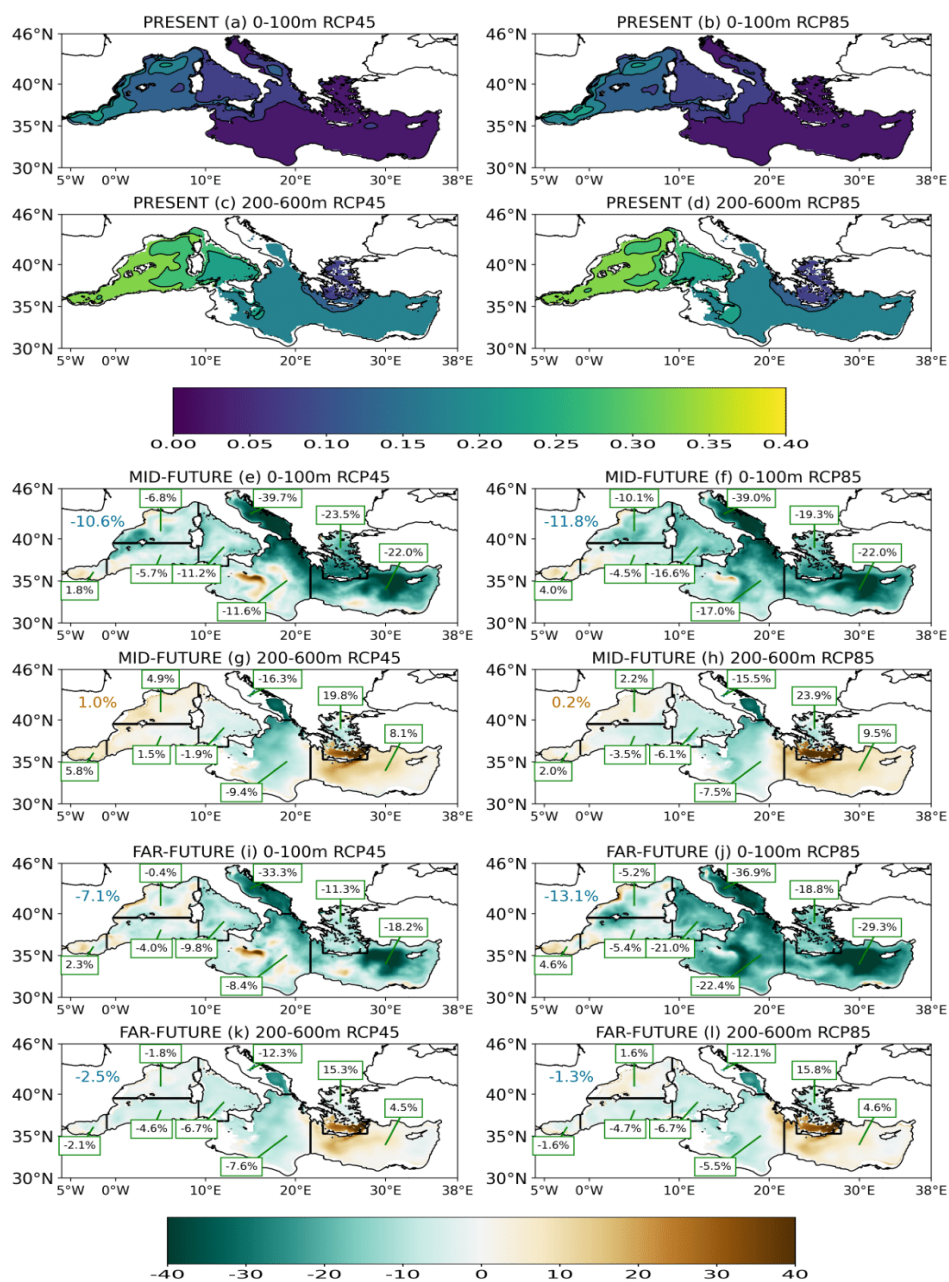
Fig. 5 - Phosphate (in mmol m⁻³) in first 0-100m and 200-600m in the present period (2005-2020, a,b, c,d), in MID future (e,f,g,h)

and FAR-FUTURE (i,j,k,l) variations in the RCP4.5 scenario (left column) and RCP8.5 (right column). The value located over

the Iberian Peninsula is the average variation on basin scale in blue/dark orange if it is negative/positive.

428
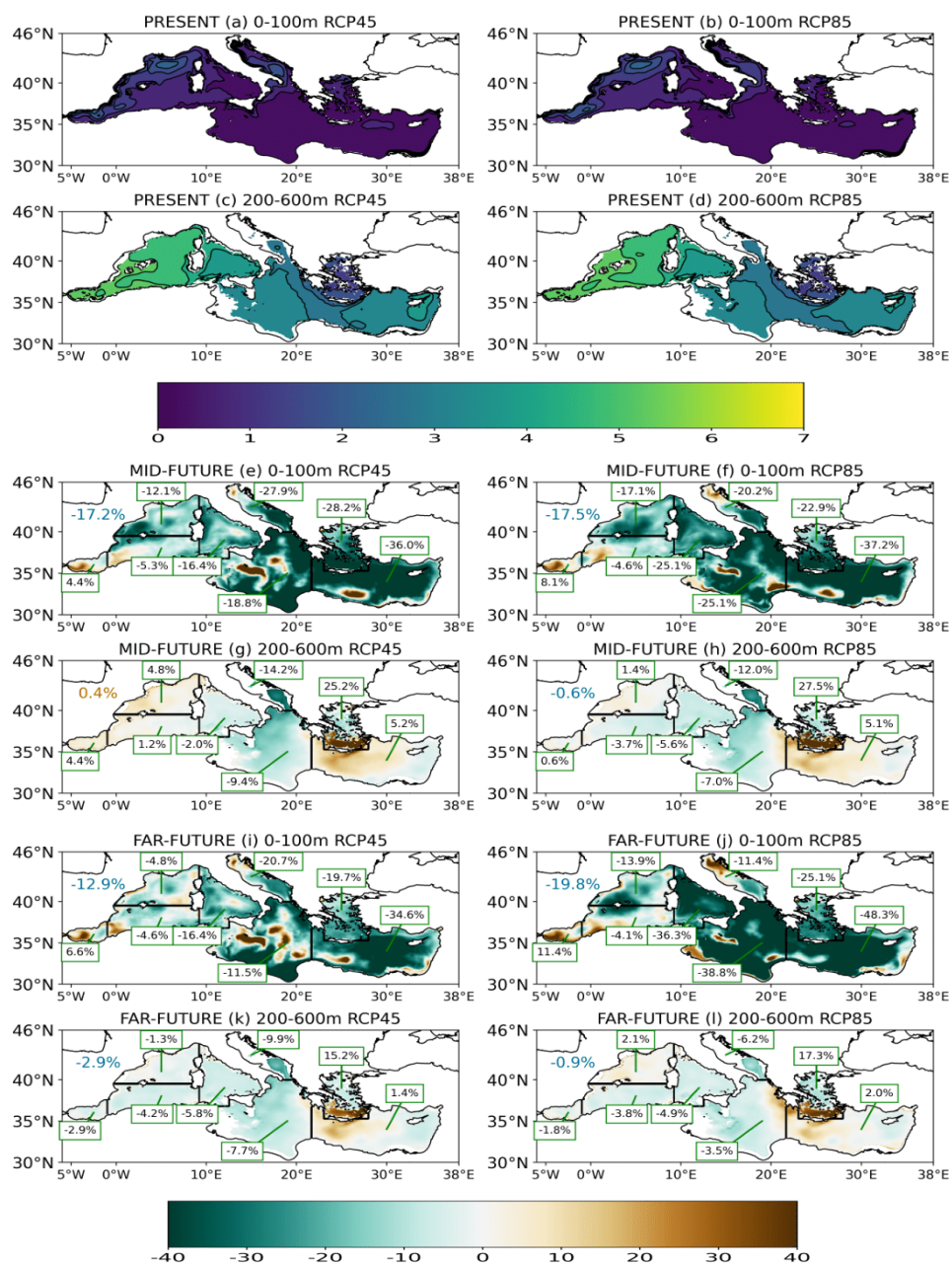
Fig.6 - as Fig.5 but for Nitrate (in mmol m⁻³)

434   The temporal evolution of the mean concentrations of PO_4 and NO_3 in the RCP4.5 and RCP8.5 simulations between 0-

435   100 m and 200-600 m in the Mediterranean Sea and its western and eastern basins for the 2005-2099 period is shown in

436   Fig. 7. In the RPC8.5 scenario, PO_4 and NO_3 concentrations within the euphotic layer of both subbasins are substantially

437   stable for the first 30 simulated years, while a marked decline occurs after 2030-2035, with values of 0.01 and 0.1 mmol

438   m^{-3} (compared to the beginning of the century) respectively, which is followed by a steady evolution of the concentration

439   values until the end of the century. The same behaviour is observed in RCP4.5, except for a recovery that takes place at

440   the end of the century in correspondence to an increase in the nutrient inflow at the Gibraltar strait (Fig. S7 in the

441   supplementary materials). The observed decline is timely in phase with the weakening of the zonal stream function

442   discussed in Fig. 4, further pointing out the importance of vertical mixing in driving the temporal variability of nutrients

443   in the euphotic layer. From this point of view, some relative maxima of both nutrient concentrations in the western and

444   eastern basins are observed for RCP4.5 in the 2015-2040 period (Fig. 5 c,d), associated with strong ocean convective

445   events taking place in the Gulf of Lions and Levantine basin (Fig. S4). The peak in both the nutrients concentration,

446   between 2055 and 2075, in RCP4.5 timely corresponds to a peak in the inflow of nutrients at the Gibraltar strait (Fig. S7).

447   Additionally, the intermediate layer of the western basin, in both scenarios, after 2035 experiences by a negative tendency

448   in the nutrient concentration which is greater than 0.01 mmol m^{-3} for PO_4 and 0.1 mmol m^{-3} NO_3, related to a reduced

449   westward transport of nutrients associated with LIW (Fig.S5).

450

451

452

453
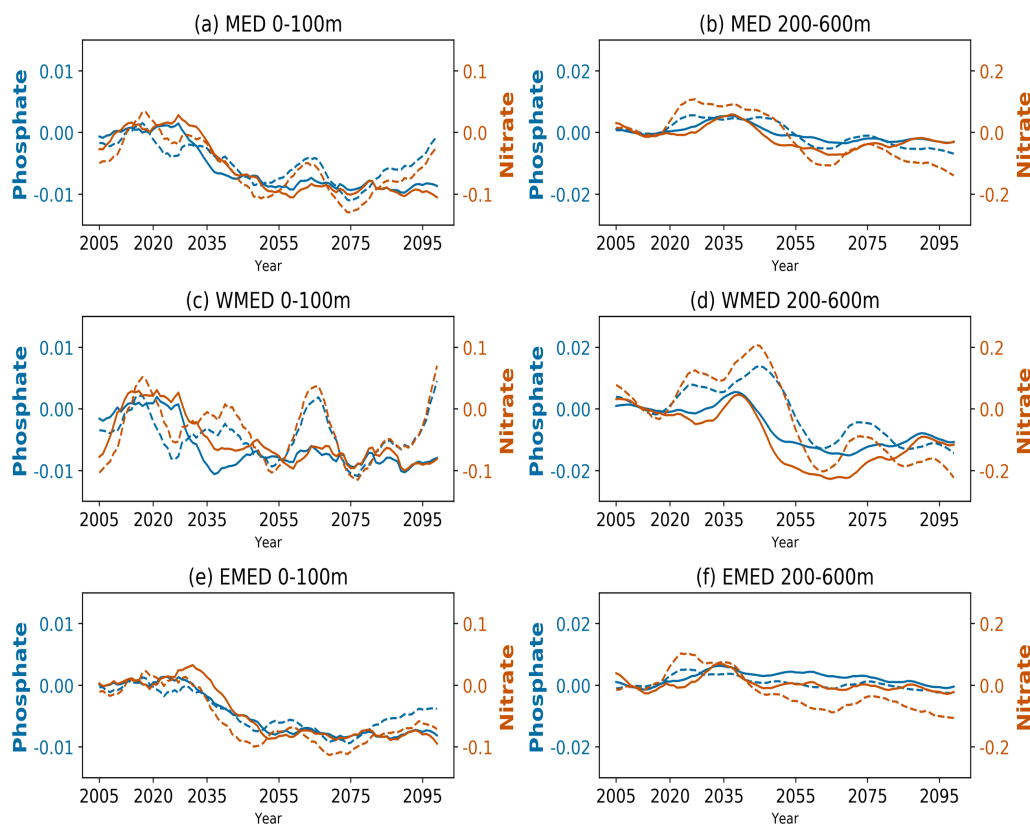
Fig.7 - Yearly timeseries for the period 2005-2099 of Phosphate (blue, in mmol m⁻³) and Nitrate (dark orange, in mmol m⁻³)
anomalies for the emission scenario RCP8.5 (solid line) and RCP4.5 (dashed line) in the Mediterranean Sea (MED, a-b),
Western Mediterranean (WMED, c-d) and Eastern Mediterranean (EMED, e-f) for the layer 0-100m (left column) and 200-
600m (right column).

458

The temporal evolution of chlorophyll-a in the two scenarios is similar to what was observed in the case of dissolved
nutrients, with a high interannual variability, a decrease after 2030-2035 of approximately 0.03 mg m⁻³ and a stable signal
until the end of the century, with RCP4.5 as the only exception, where a recovery is again observed (Fig.8). In the eastern
Mediterranean the decrease is of the same magnitude as that observed at the basin scale, while in the western basin the
chl-a signal appears substantially stable with respect to the present.
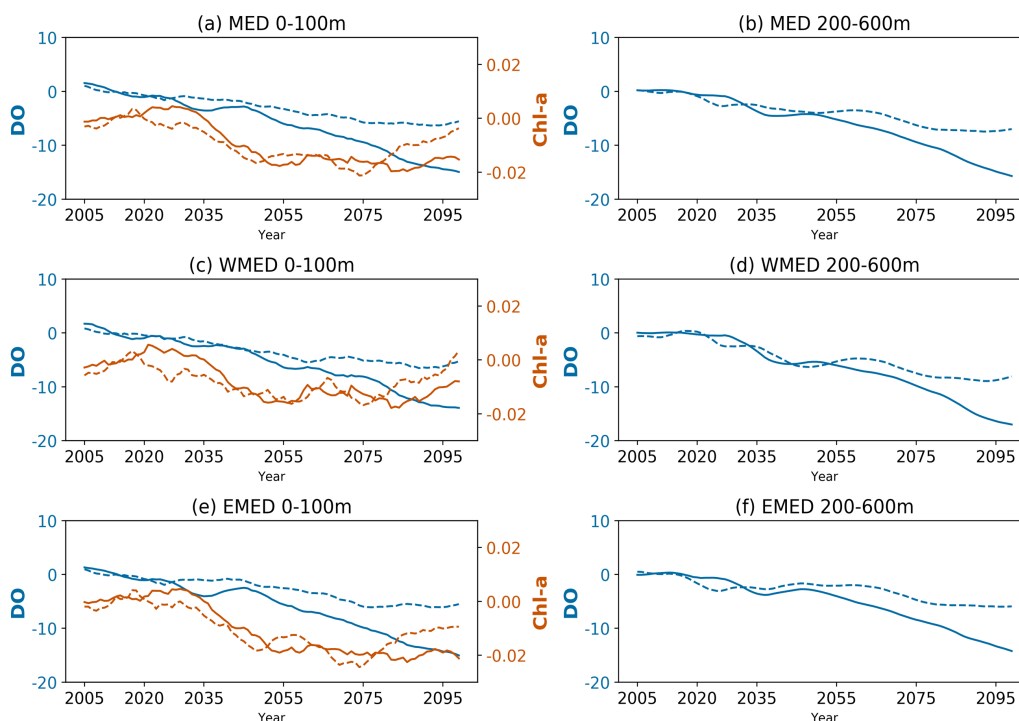
464

465   **Fig. 8 as Fig.5 but for Dissolved Oxygen (blue, in mmol m⁻³) and Chlorophyll-a (dark orange, in mg m⁻³)**

466

467   During the 21st century, a continuous decrease in the oxygen concentration is projected in both scenarios in the

468   Mediterranean Sea (Fig. 8). Under the RCP8.5 emission scenario, the concentration of the dissolved oxygen in the upper

469   layer decreases by approximately 15 mmol m⁻³, which is three times the value observed in the RCP4.5 scenario (Fig. 8).

470   The decrease in dissolved oxygen is rather uniform in both the horizontal and vertical directions in all the subbasins, with

471   values that are double in RCP8.5 (in percentages) with respect to those observed under RCP4.5 (Fig. S8, see the

472   supplementary material). For example, the decrease in the oxygen solubility in the Levantine basin in the FAR-FUTURE

473   is approximately equal to 6% under the RCP8.5 emission scenario and 3% under the RCP4.5 emission scenario. In

474   northwestern Mediterranean, these values are approximately 7% and 3% respectively. The projected decreases in both

475   scenarios are usually lower in the Alboran Sea and Southern Western Mediterranean with respect to the rest of the basin,

476   as a consequence of the damping effect driven by the oxygen values imposed at the Gibraltar Strait.

477

478   The uniform decrease in the oxygen surface concentration observed in Fig. S8 is spatially coherent with the increase in

479   the temperature shown in Fig. S4, confirming the importance of temperature in driving the solubility of the oxygen in the

480   marine environment. Moreover, we also found a decrease in the oxygen inflow (not shown) through the Gibraltar Strait

481   and an overall increase in community respiration (see the analysis related to the phytoplankton respiration in section 3.4),

482   which represent additional factors explaining the observed changes. Western subbasins and deep convection areas are the

483   regions that show the highest decrease of oxygen in the intermediate layer, with again the magnitude of the observed

484   signal depending on the scenario that is considered (Fig. S8) and related to the reduction in vertical processes intensity.

485   The effect of the increased stratification on the oxygen vertical distribution is clearly shown in Figure 9. Under RCP8.5

486 (Fig.9 a,b), the progressive decline of oxygen concentration is timely corresponding to the progressive decrease in the

487 maximum mixed layer depth (Fig. S4) and weakening of the zonal stream function (Fig.4) discussed in Section 3.2. On

488 the other hand, under RCP4.5 emission scenario, some events of deep transport of oxygen, that dumped the decline in the

489 oxygen concentration, can be recognized in both the subbasins (for example towards the end of the 21st century).
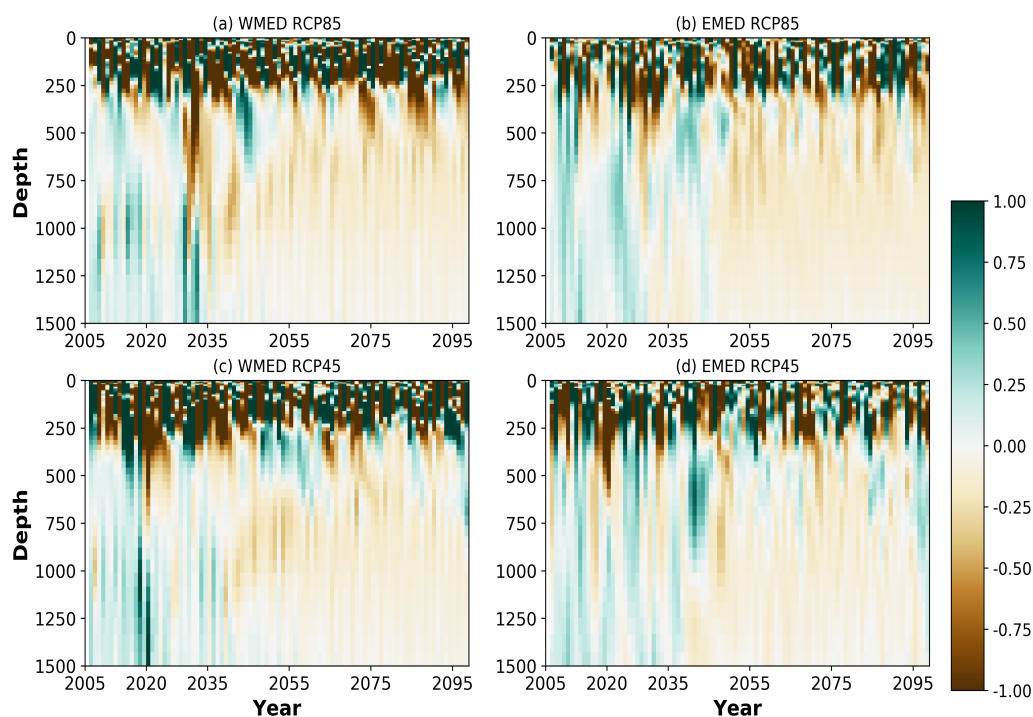
490

491 **Fig.9 Annual rate of change of Dissolved Oxygen (mmol m^{-3} year^{-1}) in the western (a,c) and eastern (b,d) Mediterranean Sea in**
492 **RCP8.5 (a,b) and RCP4.5 (c,d).**

493

494 **3.4 Spatial and temporal evolution of net primary production and living/nonliving organic matter**

495

496 The warming of the water column and the increase in vertical stratification affect the metabolic rate of ecosystem

497 processes including CO_2 fixation and community respiration. In fact, a basin-wide increase in net primary production

498 (NPP) starting after 2035 and proceeding until the end of the simulations, is projected in both the scenarios (Fig. 10). In

499 the RCP8.5 scenario the NPP increase is greater than 20 gC m^{-2} year^{-1}, which is a value that is more than double with

500 respect to the values observed in the RCP4.5 simulation.
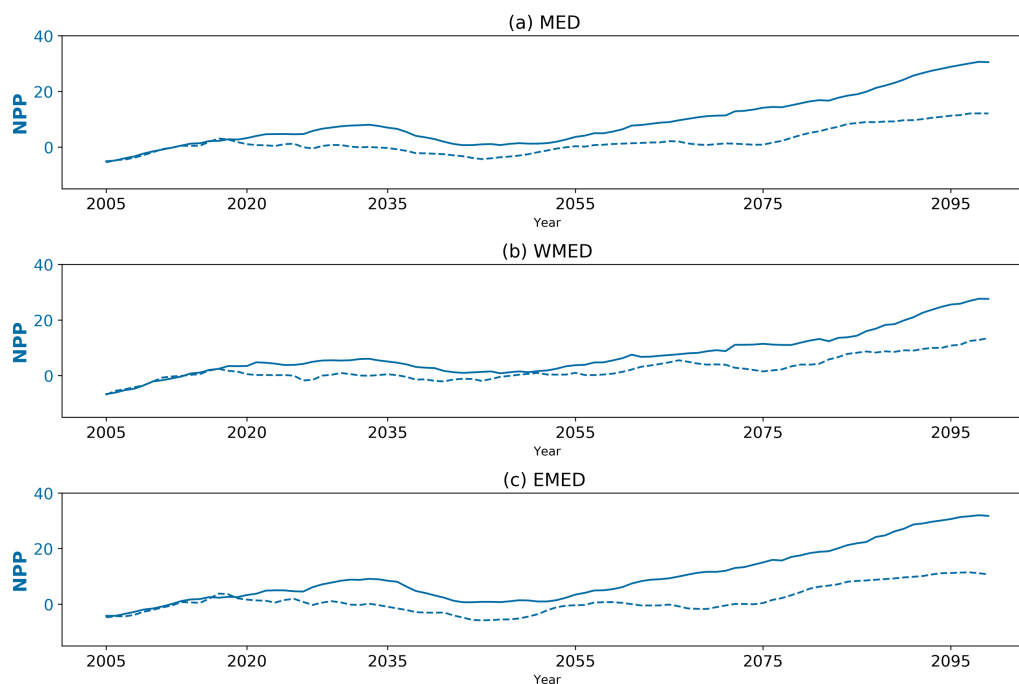
Fig.10 - Yearly time-series for the period 2005-2099 of Integrated net primary production (blue, in gC m^{-2} year^{-1}) anomalies for the emission scenario RCP8.5 (solid line) and RCP4.5 (dashed line) in the Mediterranean Sea (MED, a), Western Mediterranean (WMED, b) and Eastern Mediterranean (c) for the first 200 m. The yearly timeseries have been smoothed using 10-years running mean.

The distribution of the sign of the NPP changes is not uniform across the basin and between the simulations (Fig.12). In the MID-FUTURE in both scenarios the only areas that experience an increase in the NPP with respect to the beginning of the century are the northwestern Mediterranean, the Tyrrhenian Sea, the northern Adriatic Sea, part of the Ionian Sea and of the Levantine basin. Conversely, the rest of the Adriatic Sea, part of the Northern Ionian Sea and the Rhodes Gyre areas show negative anomalies. The Aegean Sea shows a rather opposite behaviour with a positive/negative anomaly in RCP8.5/RCP4.5. In the FAR-FUTURE, corresponding to a more pronounced warming of the basin, the NPP increase is quite uniform throughout the entire basin and is equal to 17% in RCP8.5, which is more than twice that observed in the RCP4.5 (approximately 7%). Under the RCP8.5 emission scenario there is a 7%-23% increase in NPP throughout the basin, with the highest values observed in the northwestern Mediterranean, Aegean Sea and Levantine basin (similar results, although with lower rates, were found at the end of the 21st century by Solidoro et al., 2021). Conversely, under the RCP4.5 scenario, the Adriatic Sea is still characterized by a negative anomaly (-1%), while for the rest of the basin the sign of the anomaly is positive, with the greatest values observed in the northwestern Mediterranean (approximately 12%, which is almost half of the variation observed in the RCP8.5 scenario). In both scenarios there is still a negative anomaly in the Rhodes gyre area, which is extremely weak in RCP8.5. Both negative anomalies are temporally consistent with some convective events taking place in both areas after 2080 and shown in Fig. S4.
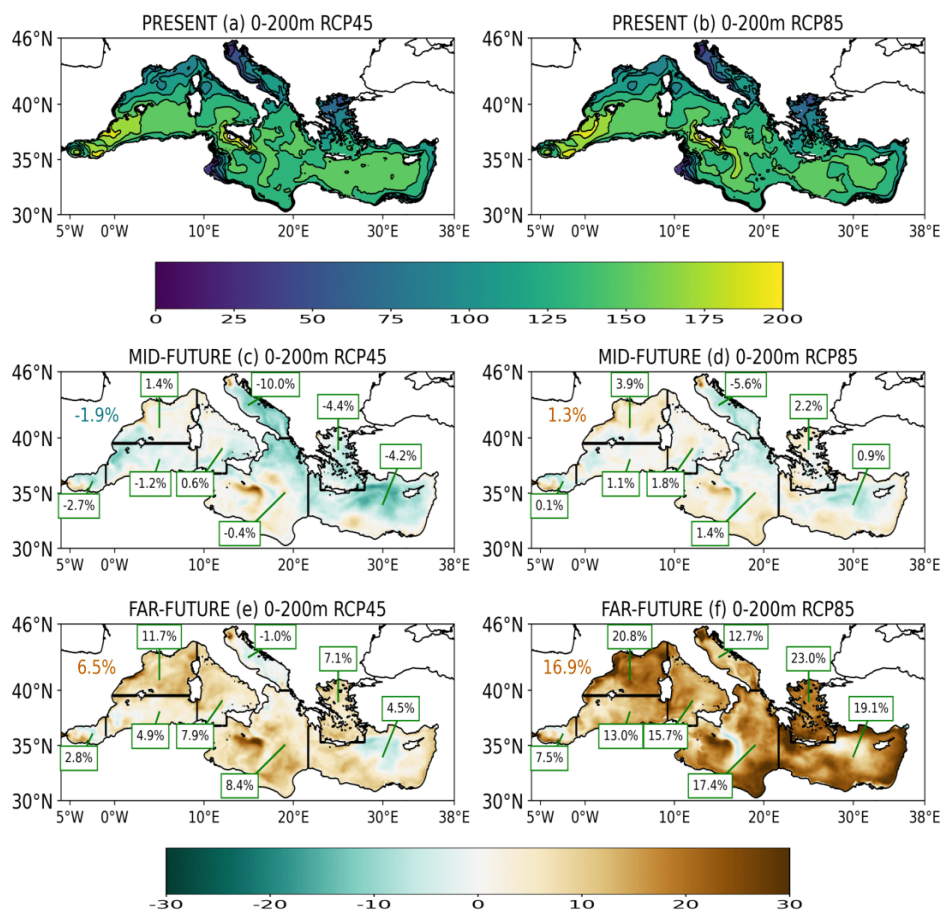
Fig. 11 - Integrated net primary production variation (in gC m⁻² year⁻¹) in first 0-200m in the present period (2005-2020, a,b), MID future (c,d) and FAR-FUTURE (e,f) variations in the RCP4.5 scenario (left column) and RCP8.5 (right column). The value located over the Iberian Peninsula is the average variation on basin scale in blue/dark orange if it is negative/positive.

As shown by Lazzari et al. (2014) and Solidoro et al. (2021), the overall warming of the water column also results in an increase in community respiration. In agreement with that, Fig. S9 (see the supplementary materials) shows the spatial distribution of phytoplankton respiration (RESP) changes in the MID-FUTURE. It is possible to observe some differences with respect to NPP. In both scenarios, there is an overall decrease in the RESP with respect to the beginning of the 21st century, which is approximately equal to -4% in the RCP4.5 and -2% in the RCP8.5. Positive signals can be observed in both scenarios in the Northern Adriatic, most of the coastal areas of the Northern Western Mediterranean, Southern Ionian and part of the Levantine basin. As previously observed for NPP, the Adriatic Sea has an overall negative anomaly together with the area of the Rhodes gyre. The northwestern Mediterranean is the only area where the variation has an opposite sign in two scenarios: it is negative (-1.4%) in RCP4.5 and positive (approximately 1%) in RCP8.5. In the FAR-FUTURE the pattern of variation is coherent with that already observed in the NPP (Fig. 11). RESP increases at the end

539   of the 21st century over the entire basin of approximately 11% in RCP8.5, again more than doubling the value observed

540   in RCP4.5 (5%). In RCP8.5, the highest values are observed in the northwestern Mediterranean (this is also true for the

541   RCP4.5 scenario), Aegean Sea and Levantine basin. Under the RCP4.5 scenario, the Adriatic Sea, with the northern part

542   as the only exception, is still characterized by a negative anomaly.

543

544   The overall increase in the respiration community and of the vertical stratification (which in turn affects the sinking

545   velocity of the particles) has a consequence on the decrease in the organic stock matter in the water column. The temporal

546   evolution of the carbon organic matter standing stock for the 2005-2099 in RCP4.5 and RCP8.5 simulations between 0-

547   100 m and 200-600 m in the whole Mediterranean and in its western and eastern basins is shown in Figure 12. The

548   behaviour of the carbon organic matter standing stock is similar to that observed in the dissolved nutrients, with a

549   substantially stable signal in the first 30 years of the 21st century and a decrease after 2030. In particular, RCP8.5 projects

550   a decline of approximately 5 mgC m^{-3} until the end of the century, while RCP4.5 shows a similar behaviour, despite a

551   recovery that is also present, in this case, at the end of the 21st century. In the intermediate layer, the decline after the

552   period 2030-2035 is approximately 0.3 mgC m^{-3} for the carbon stock, with another slight recovery observed in RCP4.5 at

553   the end of the century.

554

555   Similar dynamics are also observed for plankton (both phyto- and zoo-, Fig. 13), bacterial biomass and particulate organic

556   matter in the euphotic layer (Fig. 14). In the RCP8.5 simulation, the decrease of the phytoplankton (zooplankton) biomass

557   is approximately 2 (1.5) mgC m^{-3} and appears to be stronger in the eastern basin than in western basin. Under RCP8.5 the

558   bacterial biomass is projected to decrease at the basin scale by the end of the century by approximately 0.5 mgC m^{-3}, by

559   0.2 mgC m^{-3} in the western basin and by 0.6 mgC m^{-3} in the eastern basin. Finally, the decline in particulate organic

560   matter is approximately 1.5 mgC m^{-3} at the basin scale, approximately 1 mgC m^{-3} in the western basin and approximately

561   2 mgC m^{-3} in the eastern basin. In the intermediate layer, the decline of the bacterial biomass in the entire basin is fairly

562   uniform and continuous until the end of the 21st century, with a variation of approximately of about 0.3 mgC m^{-3} with

563   respect to the beginning of the century. For the same layer, particulate organic matter declines after the period 2030-2035

564   but successively the signal remains substantially stable and, in particular in the western basin, has a tendency to recover

565   at the end of the century. In the RCP4.5 simulation for all these biogeochemical tracers, we observe a recovery in the

566   biomass at the end of the century and the observed change is approximately 50% with respect to the RCP8.5 scenario.

567

568
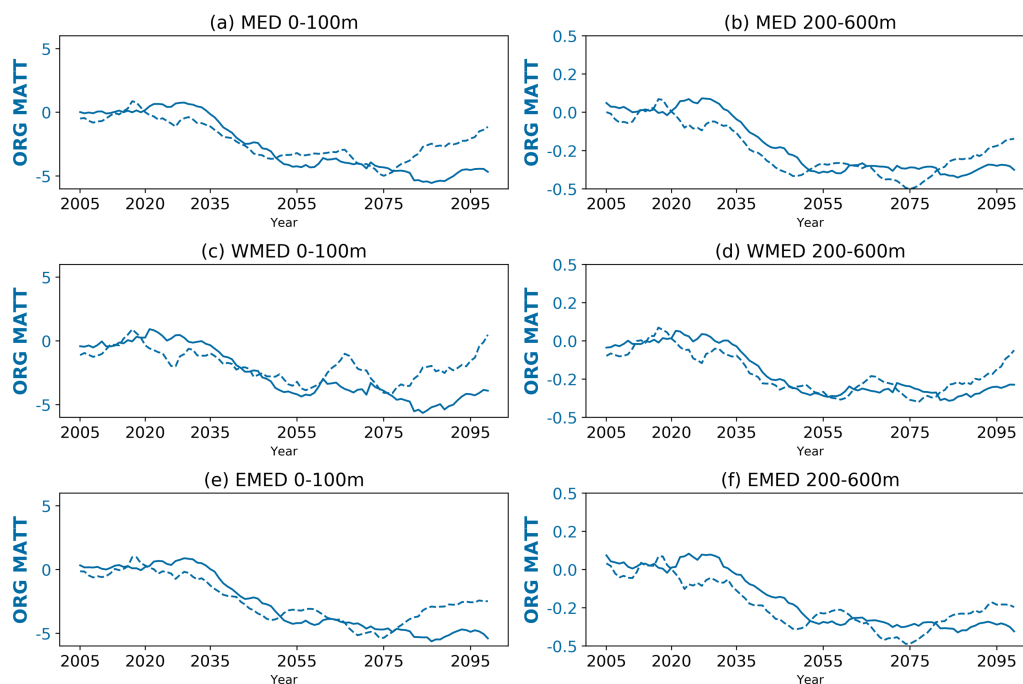
Fig. 12 - Yearly timeseries for the period 2005-2099 of Living/not Living organic Matter (in mgC m⁻³) anomalies for the emission scenario RCP8.5 (solid line) and RCP4.5 (dashed line) in the Mediterranean Sea (MED, a-b), Western Mediterranean (WMED, c-d) and Eastern Mediterranean (EMED, e-f) for the layer 0-100m (left column) and 200-600m (right column) for the 2005-2099 period. The yearly timeseries have been smoothed using 10-years running mean.

573

574

575
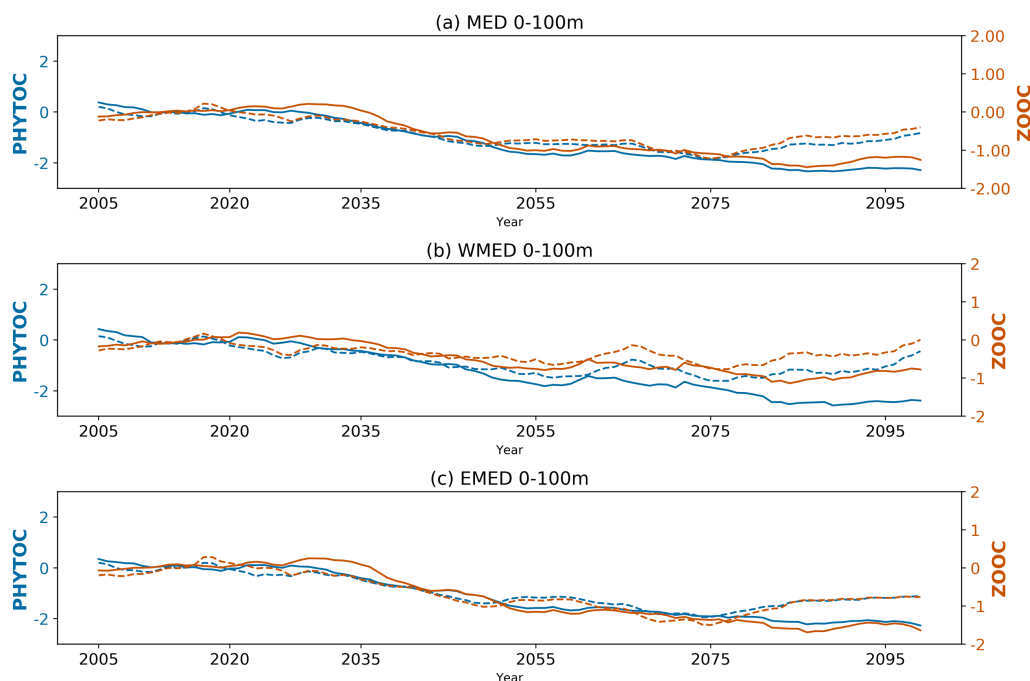
Fig. 13 - Yearly timeseries of Phytoplankton biomass (blue, in mg m^{-3}) and Zooplankton (dark orange, in mg m^{-3}) anomalies for the emission scenario RCP8.5 (solid line) and RCP4.5 (dashed line) in the Mediterranean Sea (MED, a), Western Mediterranean (WMED, b) and Eastern Mediterranean (c) for the layer 0-100m and for the 2005-2099 period.

579

580   In the two scenarios, in both MID-FUTURE and FAR-FUTURE the areas most affected by the decline of phytoplankton

581   (Fig. S10) and zooplankton (Fig. S11) biomass are mainly the sub-basins of the eastern Mediterranean Sea, namely the

582   Ionian Sea, the Aegean Sea and the Levantine basin and the Tyrrhenian Sea (only for the phytoplankton). Moreover, the

583   area of Rhodes gyre is characterized by a permanent negative anomaly (as already observed in the case of NPP and RESP,

584   consequences of the vertical convection phenomena in the area). Conversely, positive signals for both variables can be

585   observed only at the local scale in the Strait of Sicily and along the coast of the Northern Western Mediterranean (spatially

586   coherent with the positive variations of the PO$_4$ discussed in section 3.3). For the latter, the zooplankton biomass in the

587   North-Western Mediterranean increases by about 2% in the FAR-FUTURE under emission scenario RCP4.5.

588

589
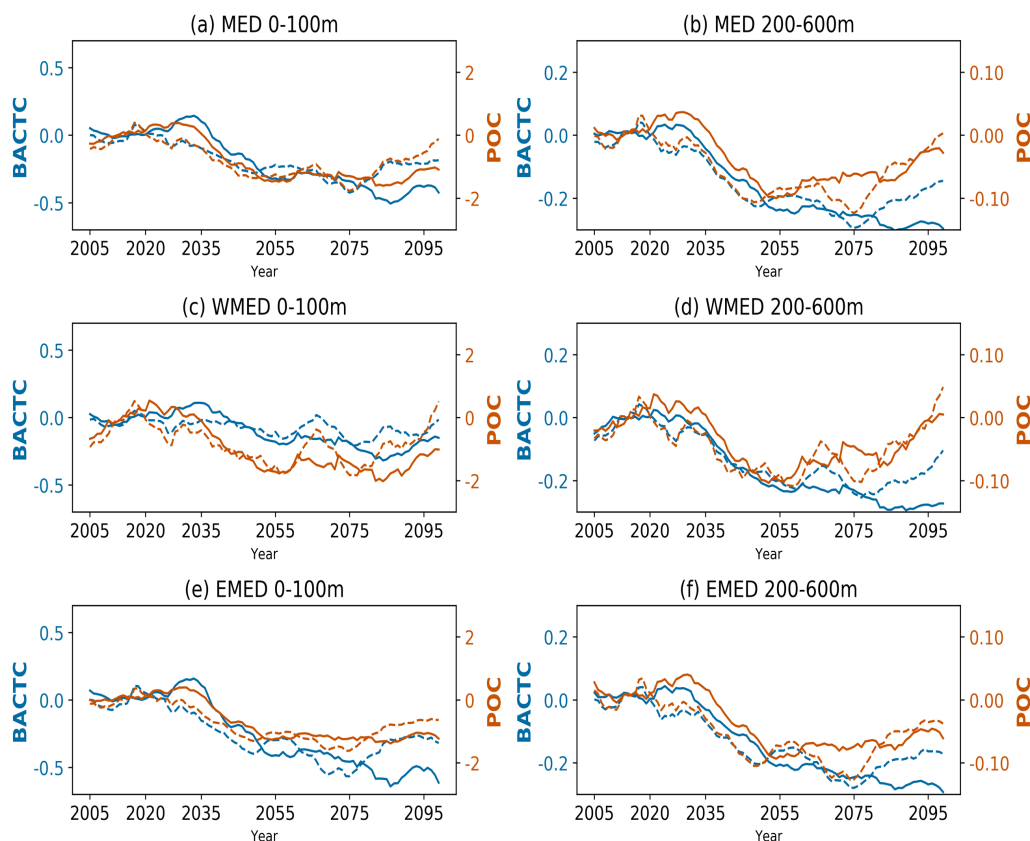
Fig.14- As Fig.8 but for bacterial biomass (blue, in mg m⁻³) and particulate organic matter (dark orange, in mg m⁻³)

591

Also, in the case of bacterial biomass (Fig. S12) and particulate organic matter (Fig. S13) the decline along the 21st century will mostly affect the euphotic and the intermediate layers of the eastern basin in both MID- and FAR-FUTURE with relative maxima observed in the Levantine basin (around 50% in the RCP8.5 scenario). This decline is related to an increase of the respiration at community level, as observed for phytoplankton (Fig. S9). However, there are some exceptions to the general decline of the bacterial biomass and particulate organic matter in the basin. For example, in the Adriatic Sea, under scenario RCP8.5, the decrease of the bacterial biomass with respect to the beginning of the century is only 1% with a slight positive anomaly appearing in the southern Adriatic at the end of 21st century (Fig. S12). In the case of particulate organic matter, the Strait of Sicily and the Northern Adriatic are characterized by a permanent positive signal in both layers and scenarios as observed before for PO_4. Moreover, in RCP4.5 simulation in the FAR-FUTURE period the North-Western Mediterranean shows an increase of the particulate organic matter content in the euphotic and intermediate layers.

603

3.4 Spatial and temporal evolution of dissolved inorganic carbon (DIC) and pH

605

606 A basin-wide continuous increase in DIC is projected until the end of the 21st century, with a stronger signal observed in

607 the RCP8.5 scenario (Fig. 15), and more specifically, in the eastern part of the Mediterranean basin. In fact, in the euphotic

608 layer, the increase in DIC with respect to the beginning of the century is approximately 150 μmol kg^{-1} under RCP8.5 in

609 the eastern basin, while it is approximately 120 μmol kg^{-1} in the western basin. Additionally, in the intermediate layer,

610 DIC increases by approximately 120 μmol kg^{-1} with respect to the beginning of the century: this value is approximately

611 the same for both the western and eastern basins and is double with respect to that observed in the RCP4.5 scenario.

612
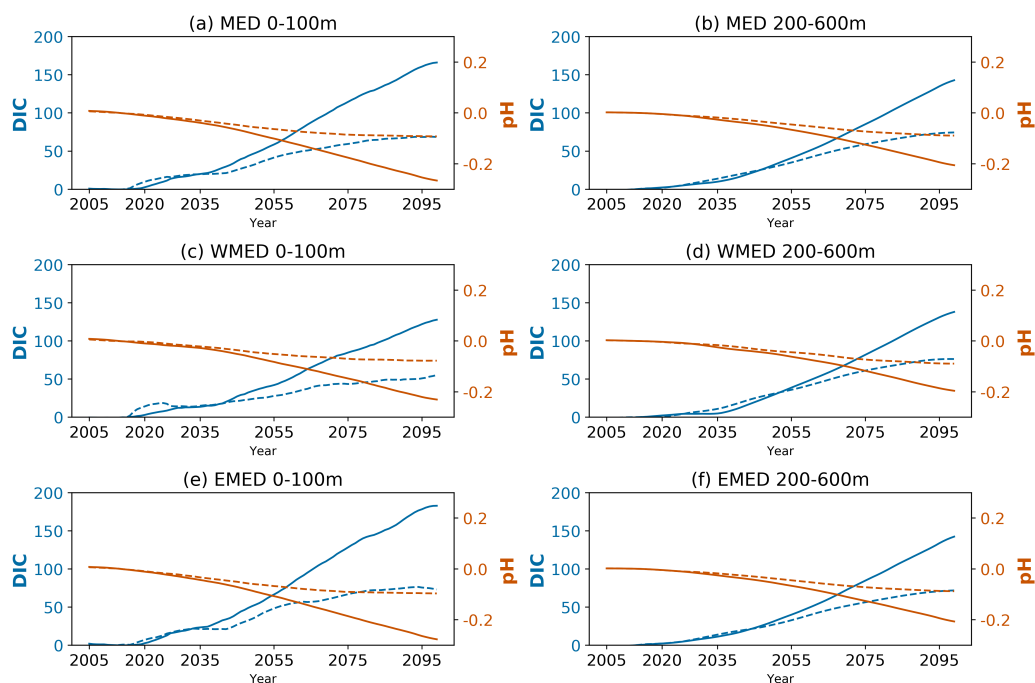
613

614 **Fig. 15 - as Fig.14 but for Dissolved Inorganic Carbon (blue, in umol kg^{-1}) and pH (dark orange)**

615

616 Although community respiration can play a role in the increase in DIC, a predominant mechanism is represented by the

617 air-sea CO_2 exchange. In fact, looking at the terms controlling the DIC increase, the air-sea CO_2 exchange shows an almost

618 balanced condition in the present-day, which is consistent with the 1999-2015 reanalysis (Melaku Canu et al., 2015), and

619 an increase throughout the 21st century as a consequence of the increase in atmospheric CO_2 (Fig. 16, a,d). The CO_2 flux

620 increase is almost linear and is fairly in the two scenarios until 2050. Then, the RCP4.5 scenario shows smoothing in the

621 second half of the century, which is consistent consistently with reduced atmospheric emissions, while the linear increase

622 persists under RCP8.5 (Fig. 16, b,e).

623

624 The two main Mediterranean sub-basins behave quite differently: the CO_2 air-sea sink is three times greater in the western

625 part than in compared to the eastern part, reflecting the influence of both DIC and temperature spatial gradients (i.e.,

626 higher values of DIC and temperature in the eastern basin). Disentangling the temperature and DIC contributions to the

627 pCO$_2$ evolution reveals that the impact of the increase in temperature on saturation accounts for 25% of the total increase,

628 while the remaining part is due to the DIC concentration increase. In the western part, a less pronounced temperature

629 effect (i.e., T increases slower in the western part) causes an undersaturation condition of pCO_2 (i.e., pCO_2^{sea} lower than

630 pCO_2^{atm} values) compared to the eastern condition triggering the much higher CO_2 absorption in the western Mediterranean.

631

632
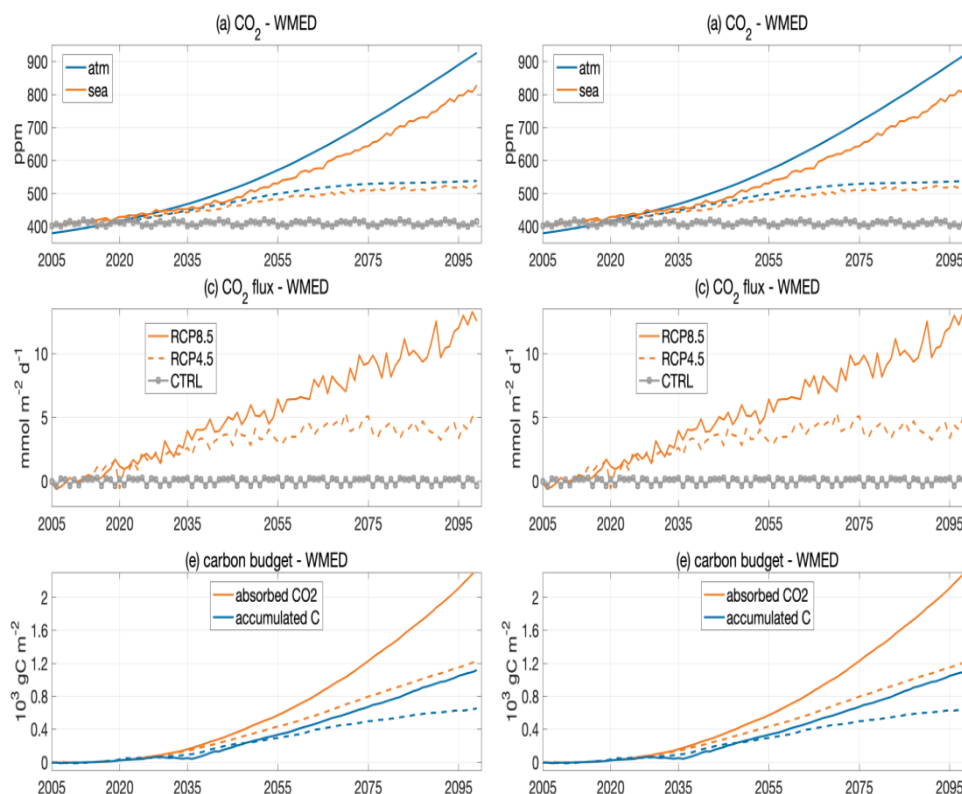
633

634 **Fig.16 - Atmospheric and marine pCO_2 (a,d), CO_2 air-sea exchange (b,e) and cumulative CO_2 absorbed and accumulated in the**

635 **water column during the scenario simulations (c,f) in the western (a,b,c) and eastern (d,e,f) Mediterranean Sea. Two scenarios**

636 **RCP45 (dashed line) and RCP85 (continuous line) and control simulation (CTRL, gray line) are reported.**

637

638 As a result of the air-sea CO_2 sink, the RCP8.5 scenario shows a steady DIC accumulation after 2030 with values of 2

639 μmol kg^{-1} year^{-1} in the first 600 m (500 m) of the water column for the western basin (eastern basin; Fig. 17).

640

641 The increase in DIC in the upper layer is approximately 1.5% and 2.5% in the western and eastern basins, respectively,

642 in the MID-FUTURE, and 5% and 7% in the FAR-FUTURE (not shown). In the 200-600 m layers, the DIC increase

643 follows the same pattern as that in the upper layer, but with smaller changes (i.e., approximately 1-2% less). Then, while

644 the DIC increase does not impact the water column below 1200 m in the western basin, DIC still accumulates until 2000

645 m in the eastern basin at a rate of almost 0.5 μmol kg^{-1} year^{-1} (Fig. 17). Occasional events of deep transport of DIC can

646 be recognized (e.g. around the years 2035, 2045, 2085 and 2095, similar to what observed in case of oxygen in Fig.9) and

647   the water column results enriched down to 1000-1500 m with a rate of approximately 1 μmol kg^{-1} year^{-1}. In the surface

648   layer (i.e., first 50-100m), the interannual variability in atmospheric conditions (i.e., specific annual wind and temperature

649   seasonal cycles triggering the CO$_2$ fluxes) and winter mixing produces an irregular succession of positive and negative

650   annual changes, which can partially hide the long-term effect of the increase in atmospheric pCO2. Thus, the cumulative

651   sum of the CO$_2$ absorbed through air-sea exchanges and of the carbon accumulated in the water column (Fig. 16, c,f panel)

652   highlight the different behaviour of the two main subbasins. The western basin absorbs much more atmospheric CO$_2$ than

653   the eastern basin, with even larger differences in the RCP8.5 scenario. By the end of the RCP8.5 scenario, we observe

654   1.8 PgC of atmospheric CO$_2$ sink in the western subbasin while only 1 PgC in the eastern subbasin, consistent with what

655   the estimates discussed in Solidoro et al. (2021).

656

657   However, the fate of the absorbed carbon is quite different: the western basin accumulates only 0.85 PgC by the end of

658   RCP8.5, while 1.7 PgC are retained in the water column of the eastern basin. As shown in Figure 17 (lower panel) for the

659   RCP8.5 scenario, the eastern basin accumulates almost 2 moles of carbon for each atmospheric CO$_2$ mole absorbed (up

660   to 3 in the RCP4.5), while it is less than 0.5 for the western basin. The different efficiency is eventually triggered by the

661   thermohaline circulation change: the western Mediterranean carbon is partly exported to the northern Atlantic Ocean,

662   while an increased quota of carbon input from rivers and across the Sicily channel are retained in the eastern basin together

663   with the atmospheric CO$_2$ sink after the weakening of the thermohaline circulation (Fig.4). The RCP4.5 scenario shows

664   similar dynamics to RPC8.5, with rates of CO$_2$ absorption (Fig. 17) and of DIC accumulation almost halved, and the

665   impact of the interannual variability on surface layer dynamics much more amplified (not shown). As a result, the total

666   sequestered atmospheric CO$_2$ equals to 0.8 and 0.25 PgC in the western and eastern basins, while the increases of the

667   carbon pool are 0.5 PgC and 0.9 PgC, respectively.

668
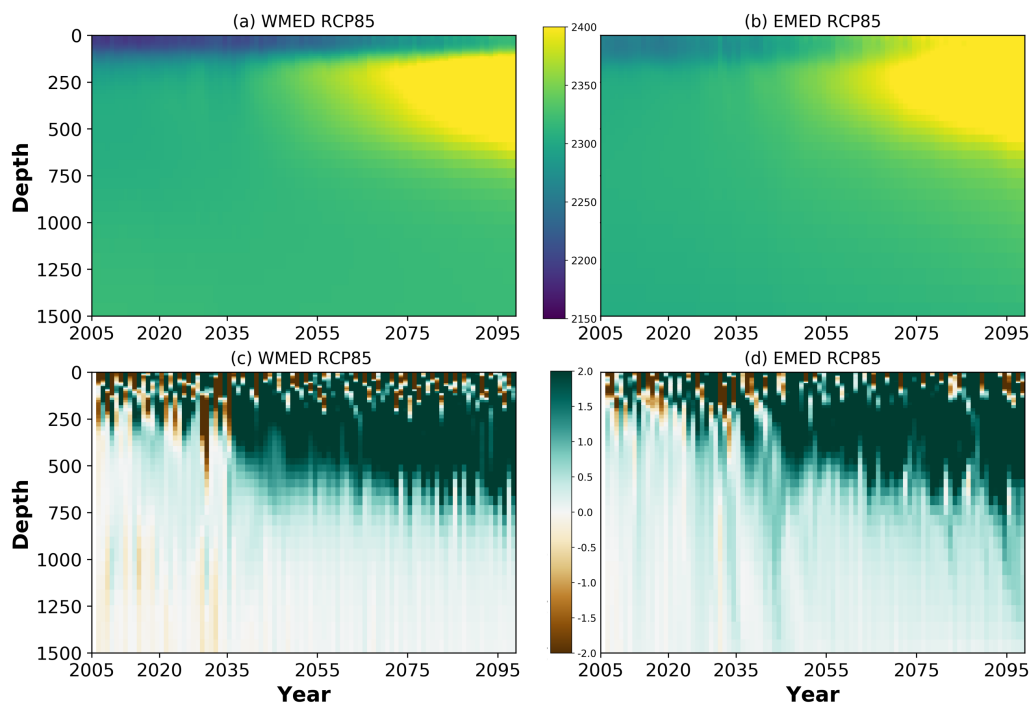
Fig. 17 - Hovmoeller diagram of DIC (umol kg⁻¹, panel a,b) and annual rate of change of DIC (umol kg⁻¹ year⁻¹, panel c,d) in the western (a,c) and eastern (b,d) Mediterranean Sea in RCP8.5 scenario.

Consequently, to the CO₂ invasion and DIC increase, the change in the carbonic acid equilibrium causes a generalized decrease in pH, as also shown in Solidoro et al. (2021) in the case of the A2 scenario. The change in pH, which is very well correlated in time and space with the DIC change, is approximately 0.25 units by the end of the RCP8.5 scenario (Fig. 18), but some differences are visible among subbasins. Larger decreases in pH are projected in the upper layer of the Tyrrhenian Sea, Adriatic Sea and Aegean Sea and in the 200-600 m layers of the Tyrrhenian Sea, Ionian Sea and Aegean Sea in the FAR-FUTURE (Fig. 18). RCP4.5, which follows RCP8.5 evolution until the MID-FUTURE period, presents a decrease in pH that does not exceed 1.1-1.2% in both the upper and 200-600 m layers by the end of the century.

pH

681
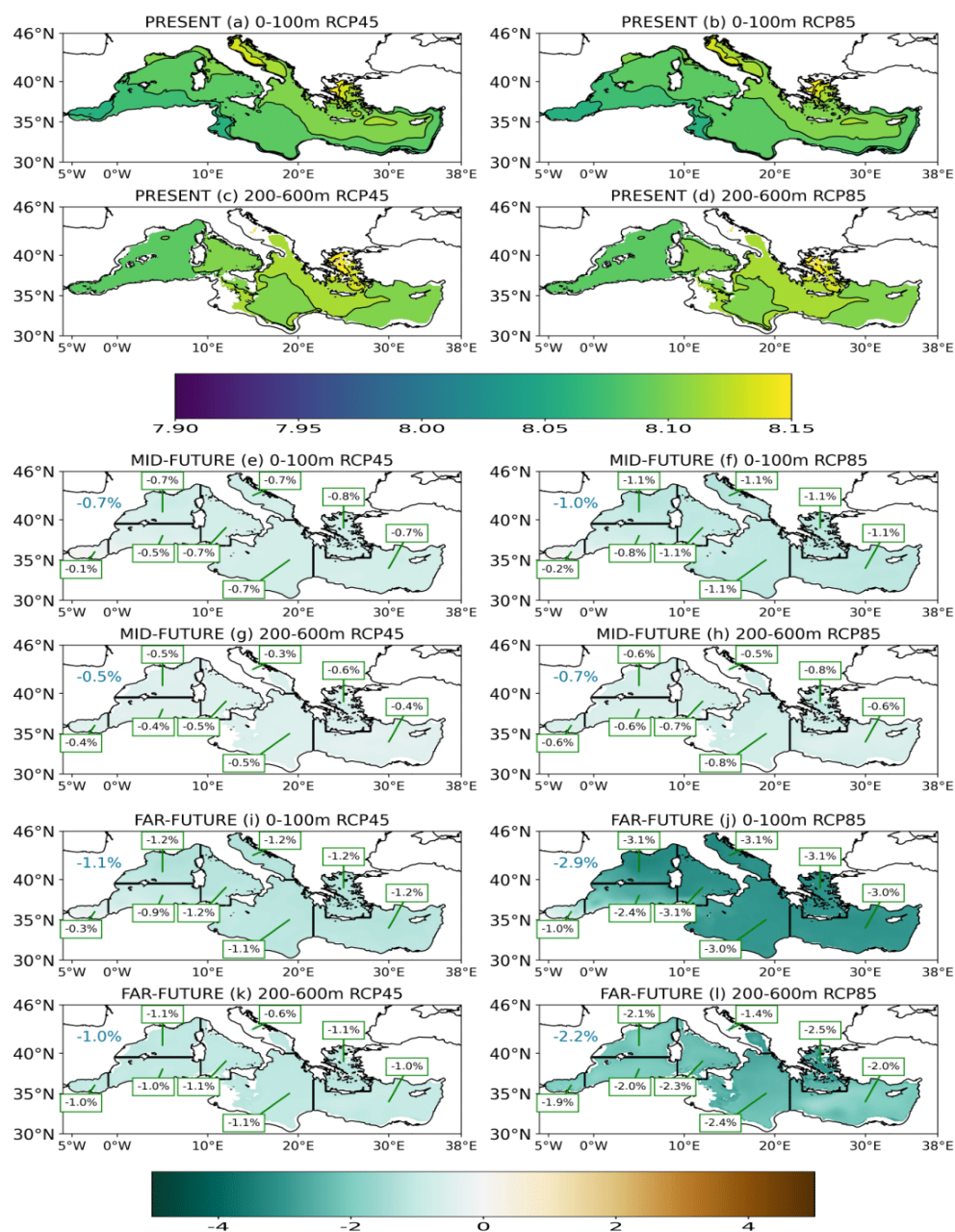
Fig. 18 – pH in first 0-100m and 200-600m in the present period (2005-2020, a,b, c,d), MID future (e,f,g,h) and FAR-FUTURE
682
(i, j,k,l) variations in the RCP4.5 scenario (left column) and RCP8.5 (right column). The value located over the Iberian
683
Peninsula is the average variation on basin scale in blue/dark orange if it is negative/positive.
684

685

686

4. Discussions and conclusions

688

In this study we use the coupled physical-biogeochemical model MFS16-OGSTM-BFM to simulate the biogeochemical dynamics of the Mediterranean Sea during the 21st century under the two emission scenarios RCP8.5 and RCP4.5, and to assess some climate-related impacts on the marine ecosystems of the basin.

692

To the best of the authors' knowledge this work is the first to focus on the Mediterranean Sea based on the projection of the biogeochemical tracers dynamics under two different emission scenarios and with horizontal and vertical resolutions (1/16° and 70 vertical levels) that are higher than those of previous works available in the scientific literature that focuses on the area (e.g Lazzari et al., 2014; Macias et al., 2015; Richon et al., 2019; Pagès et al., 2020; Solidoro et al., 2021). The use of eddy resolving higher horizontal and vertical resolutions allows a more detailed representation of the vertical mixing and ocean convection processes, which play a fundamental role in the ventilation of the water column and in the nutrient supply into the euphotic layer of the basin (Kwiatkowski et al., 2020). Moreover, the higher resolution represents an advantage for the future assessment of climate change impacts on specific organisms, habitats or target areas.

701

The analysis of the thermohaline properties and circulation of the Mediterranean Sea under emission scenarios RCP4.5 and RCP8.5 showed an overall warming of the water column and a weakening of the thermohaline circulation cell, with different parts of the basin being characterized by contrasting saltening and freshening conditions as a function of the considered scenarios. Moreover, we observe an overall weakening of the open ocean convection in the most important convective areas of the basin, with the only exception of the Aegean Sea, where episodes of deep convection similar to the EMT could be observed at the end of the 21st century (see also Adloff et al., 2015). All the projected changes are in agreement with those already depicted in recent model studies (e.g. Somot et al., 2006; Adloff et al., 2015; Waldman et al., 2018; Soto-Navarro et al., 2020).

710

A comparison of the model outputs with available data in the present climate, together with previous studies performed with the same model system, support the conclusion that the coupled model MFS16-OGSTM-BFM has reasonably good ability in reproducing the main biogeochemical features of the Mediterranean Sea and can be used as a tool for assessing the future biogeochemical dynamics of the basin and its changes in response to climate change. The use of bias-removing protocol, often advocate as a good practice in climate studies, but rarely implemented in biogeochemical or ecosystem projections (Solidoro et al., 2021), add further robustness to our results.

717

Our projections for the biogeochemical tracers and processes at the end of the 21st century shows several signals that are in agreement with previous studies. The decrease in dissolved nutrients in the euphotic layer of the basin and in the intermediate layer of the central part of the Mediterranean Sea, the increases in the net primary production and respiration, the decline of the stocks of particulate carbon biomass (including phytoplankton, zooplankton, bacterial biomass and particulate organic matter), the uniform surface and subsurface deoxygenation of the water column simulated in the RCP8.5 scenario, are globally in agreement with the conclusions of previous regional and global case studies (e.g Hermann et al., 2014; Lazzari et al., 2014; Macias et al., 2015; Moullec et al., 2019; Richon et al., 2019; Pagès et al.,

725   2020; Kwiatkowski et al., 2020; Solidoro et al., 2021). We also observe an increase in the dissolved inorganic carbon

726   content and acidity of the water column (Solidoro et al., 2021). The magnitude of the observed changes has been shown

727   to be scenario-dependent with the largest deviations from the present climate state observed in the RCP8.5 (worst-case)

728   scenario.

730   The decline in many biogeochemical tracers in the euphotic layer begins in the 2030-2035 period, in correspondence to

731   the weakening of the thermohaline circulation in the basin (Fig. 4), and it is particularly marked in the eastern basin. This

732   shows that the modification of the circulation resulting from future climate scenarios has substantial effects on the

733   biogeochemical properties of the basin. Changes in the thermohaline circulation of the basin also explain the increase in

734   the nutrient concentration in the intermediate layer of the Levantine basin, which is a result of the weakening of the

735   westward transport of nutrients through the Strait of Sicily (Fig.S5). Nevertheless, the increase in the concentration of

736   nutrients in the intermediate layers of both the western and Levantine basins can be also traced back to the reduced vertical

737   mixing resulting from the increase in the vertical stratification (Somot et al., 2006; Adloff et al., 2015; Richon et al.,

738   2019). The decline in the dissolved nutrients at the surface is comparable with that observed in Richon et al. (2019), the

739   latter also projecting an overall increase in the concentration of both nutrients at the surface after 2050, which is ascribed

740   by the authors to river and Gibraltar inputs that are not constant over time (as in our case) but are based on a global climate

741   scenario simulation. As highlighted by Richon et al. (2019), the sensitivity of the biogeochemical fluxes at the river loads

742   and Gibraltar exchanges is of paramount importance, and surely worthy of further investigation.

744   As already discussed in the introduction, many recent studies in the Mediterranean region have shown a different response

745   of integrated net primary production to climate change. In fact, this response may vary according to the sensitivity of the

746   assumptions (model equations) for primary production and recycling processes to changes in temperature (Moullec et al.,

747   2019). Our projections of primary productivity and biomass dynamics show how the warming of the water column and

748   consequent stratification have a direct impact on the ecosystem functioning by increasing the metabolic rates. Similar to

749   the results obtained in Lazzari et al. (2014) and Solidoro et al. (2021), the increase in metabolic rates augments both

750   primary productivity and respiration, but with the net effect of reducing living and nonliving particulate organic matter,

751   as suggested from theoretical considerations in O'Connor et al. (2011). The decoupled formulation of carbon uptake and

752   net growth in the BFM model induces a further mechanism related to how carbon is channelled in the food web. In fact,

753   the decrease in biomass is partially compensated by an increase in dissolved organic matter production in the basin by

754   the end of the century (Solidoro et al., 2021; results not shown here).

756   Surface and intermediate layer deoxygenation, which are driven by the projected warming and by the increase in the

757   respiration and reduced oxygen inflow in the Gibraltar Strait, is rather uniform throughout the basin (approximately -15

758   mmol m^{-3} in the worst scenario at the end of 21st century), showing that in this case, the climate forcing acts almost

759   uniformly over the Mediterranean Sea. Our basin-wide deoxygenation is comparable to trends observed on the global

760   scale CMIP6 simulations (Kwiatkowski et al., 2020) and on the Mediterranean scale by Powley et al. (2018). The latter,

761   using a box model, found a decrease in the oxygen content of the intermediate layer in the range of 2-9% as a consequence

762   of different projected changes in the solubility (due to the temperature increase) and in the thermohaline circulation of

763   the basin. Furthermore, our results show that deoxygenation is higher in the eastern than the western basin, where the

764   Atlantic boundary condition might have dumped the deoxygenation trend, and in several coastal areas such as the

765   Northern Adriatic (until -25 mmol m^{-3}). As also observed by Powley et al. (2018), the main driver of deoxygenation is

766   the change in solubility, whereas changes in the circulation (i.e., weakening of the thermohaline circulation) should not

767   substantially affect deep ventilation, and it is unlikely to reach hypoxia conditions in the deep layer of the basin by the

768   end of the century. On the other hand, the greatest threat considering the oxygen water content might be linked to local

769   conditions of surface warming (such as in coastal areas).

770

771   This difference in the response to climate change between the western and eastern basins has been also observed for the

772   dissolved inorganic carbon accumulation and indeed reflects the influence of the exchanges in the Gibraltar Strait. Results

773   show that the western basin, while adsorbing greater quantities, accumulates only a half of the atmospheric carbon stored

774   by the eastern basin (1.85 PgC) because in the former the carbon is partly exported to the northern Atlantic Ocean, while

775   in the latter, it is also affected by a more intense reduction of the thermohaline circulation and therefore in the vertical

776   transport processes, the carbon is retained together with the atmospheric CO_2 sink. The overall accumulation of the CO_2

777   in the basin resulted in an acidification of the Mediterranean water with a decrease of pH of approximately 0.25 units,

778   which is slightly lower than the value (0.3) projected on a global scale (Kwiatkowski et al., 2020). Additionally, in our

779   case, the use of a high resolution for the biogeochemical projections has shown that in many coastal areas the observed

780   acidification is lower by approximately 8% with respect to the open ocean due to damping effects of alkalinity input from

781   the rivers (not shown here).

782

783   Similar to all previous modelling cited studies (e.g Lazzari et al., 2014; Macias et al., 2018; Richon et al., 2019; Pagès et

784   al., 2020), some sources of uncertainties for our projections need to be considered. As discussed before, MFS16

785   adequately reproduces the distribution of key physical properties and the thermohaline circulation of the basin. On the

786   other hand, recent studies based on multi-model ensembles (Adloff et al., 2015; Richon et al., 2019; Soto-Navarro et al.,

787   2020) have suggested that atmospheric forcing and boundary conditions can strongly affect the dynamics of the basin,

788   particularly the vertical mixing, which plays a primary role in the distribution of nutrients in the euphotic layer, therefore

789   affecting the dynamics of low trophic levels. Additional sources of uncertainties in the modelling framework can be traced

790   to the BFM biogeochemical model. For instance, in the present climate the model clearly overestimates the chlorophyll-

791   a at the surface and, even more, the oxygen concentration below 200 m. These overestimations can be propagated by the

792   integration into the future projections.

793

794   Furthermore, the set-up of the boundary conditions, namely the atmospheric deposition at the surface, the rivers nutrient

795   loads and the vertical profiles in the Atlantic boundary can be very critical, especially in the land-locked Mediterranean

796   basin. In fact, in both RCP4.5 and RCP8.5 simulations we used present-day phosphate and nitrogen deposition, but

797   potential improvements could be achieved by the inclusion of more accurate deposition information derived from CMIP6

798   global estimates for the 21st century (O'Neill et al., 2016). Moreover, the biogeochemical dynamics of the Mediterranean

799   Sea is influenced by aerosol deposition (e.g. Richon et al., 2018, 2019), and thus, possible future changes in the deposition

800   of aerosols could influence the biogeochemistry of the basin and the nutrients concentration at the surface projected for

801   the 21st century and depicted in Section 3.3.

802

803   Similarly, the lack of river nutrient load projections under the prescribed emission scenarios can affect the projected

804   nutrient budget of the Mediterranean basin. We used a climatology derived from the Perseus project (see Section 2.3),

805   which is, to our knowledge, the most reliable information. Indeed, it is reasonable to assume that land-use and runoff

806   changes might impact future nutrient loads, although the magnitude and even the sign are presently unknown. Our river

807   runoff was based on projections (Gualdi et al., 2013; Section 2.1) which estimated an average decrease by the end of the

808   21st century. Thus, the increase of nutrients observed in Fig. 9 and Fig. 10 in the Northern Adriatic and several coastal

809   areas of the western basin can be partially related to the mismatch between a constant nutrient load and a decreasing

810   runoff. However, it might worth to remember that the amount of nutrients entering the basin through its boundaries

811   ultimately depends on the economic policies and land used/coverage scenarios and therefore they may be intrinsically

812   subjective.

813

814   With DIC as the only exception, for the 21st century, we used a single vertical profile based on the present-day condition

815   data and no future evolutions are considered for the boundary conditions at the Gibraltar Strait. If this approach allows to

816   point out the effects of the changes in the basin circulation on the nutrient budgets, it could miss the influence on nutrients

817   or other biogeochemical properties of a possible different future evolution of the exchanges in the Gibraltar Strait due to

818   changes in the tracer concentrations in the Atlantic Ocean. Recent physical simulations have shown an increase of 3.7%

819   in the surface flow at the Gibraltar Strait, which could imply an increase in the inflow of nutrients in the surface layer at

820   Gibraltar Strait (Richon et al., 2019; Pagès et al., 2020), thereby eventually damping the decrease in the nutrient

821   concentration at the surface projected for the 21st century. As previously observed, this could explain the observed

822   differences among different studies that analysed future projections of the biogeochemistry of the basin.

823

824   To conclude, we demonstrated that the methodology and results here presented, provide a robust picture of the evolution

825   of the Mediterranean Sea biogeochemistry for the 21st century. Clearly, the new generation of Regional Earth System

826   Coupled Models (RESM), with eddy resolving ocean models such the one exploited here, may partially reduce the

827   limitations of using external (and possibly misaligned) sources of information for atmospheric and land input to the ocean.

828   Indeed, by directly resolving the coupling between the Mediterranean Sea, the regional atmospheric domain and the

829   hydrological component, a regional earth system coupled model (e.g., as in Sitz et al., 2017, and Reale et al., 2020a)

830   allows the simulation of the different components of the climate system at the local scale, including aerosol and river

831   loads.

832

833   **Acknowledgements**

834   M. Reale has been supported in this work by OGS and CINECA under HPC-TRES award number 2015-07 and by the

835   project FAIRSEA (Fisheries in the Adriatic Region - a Shared Ecosystem. Approach) funded by the 2014 - 2020 Interreg

836   V-A Italy - Croatia CBC Programme (Standard project ID 10046951). This work has been partially supported by the

837   Italian PRIN project ICCC (Impact of Climate Change on the biogeochemistry of Contaminants in the Mediterranean

838   Sea). We acknowledge the CINECA consortium for providing the computational resources through the IscraB project

839   "Scenarios for the Mediterranean Sea biogeochemistry in the 21st century" (MED21BIO) and the IscraC DYBIO,

840   EMED18 and MEDCLI16.

841

842   **Data availability**

843   Data produced in the numerical experiments are available through the portal dds.cmcc.it

844

845   **Author contribution**

846 GC, PL, SS and CS conceived the study. They designed the experiments together with TL and MR. MR, GB and TL
847 performed the numerical simulations. MR, GC, SS, TL and PL performed the analysis of the simulation results. MR
848 prepared the first draft of the manuscript under the supervision of SS, GC and CS and with the contribution from all the
849 authors. All the authors discussed the results and contributed to the revision of the manuscript.
850

851 **Competing interest**
852 The authors declare that they have no competing interests.
853

854 **References**
855

856 Adloff, F., Somot, S., Sevault, F. et al. : Mediterranean Sea response to climate change in an ensemble of twenty first
857 century scenarios. *Clim Dyn* 45, 2775–2802. https://doi.org/10.1007/s00382-015-2507-3, 2015
858

859 Auger P.A., Ulses C., Estournel C., Stemman L., Somot S. and Diaz F. : Interannual control of plankton ecosystem in a
860 deep convection area as inferred from a 30-year 3D modeling study: winter mixing and prey/predator in the NW
861 Mediterranean. Progress in Oceanography, 124, 12-27, DOI: 10.1016/j.pocean.2014.04.004, 2014
862

863 Bethoux, J. P., Morin, P., Chaumery, C., Connan, O., Gentili, B., and Ruiz-Pino, D.: Nutrients in the Mediterranean Sea,
864 mass balance and statistical analysis of concentrations with respect to environmental change, Mar. Chem., 63, 155–169,
865 1998
866

866 Buga L., G. Sarbu, L. Fryberg, W. Magnus, K. Wesslander, J. Gatti, D. Leroy, S. Iona, M. Larsen, J. Koefoed Rømer,
867 A.K. Østrem, M. Lipizer, A. Giorgetti : EMODnet Thematic Lot n° 4/SI2.749773 EMODnet Chemistry Eutrophication
868 and Acidity aggregated datasets v2018 doi: 10.6092/EC8207EF-ED81-4EE5-BF48-E26FF16BF02E, 2018
869

870 Butenschön, M., Lovato, T., Masina, S., Caserini, S., and Grosso, M.: Alkalinization Scenarios in the Mediterranean Sea
871 for Efficient Removal of Atmospheric CO2 and the Mitigation of Ocean Acidification. *Frontiers in Climate*, 3, 14. 2021
872

873 Canu, D. M., Ghermandi, A., Nunes, P. A., Lazzari, P., Cossarini, G., and Solidoro, C.: Estimating the value of carbon
874 sequestration ecosystem services in the Mediterranean Sea: An ecological economics approach. *Global Environmental*
875 *Change*, 32, 87-95. 2015
876

877 Claustre, H., Morel, A., Hooker, S. B., Babin, M., Antoine, D., Oubelkheir, K., Bricaud, A., Leblanc, K., Quéguiner, B.,
878 Maritorena, S.: Is desert dust making oligotrophic waters greener? Geophys. Res. Lett., 29, 1–4,
879 https://doi.org/10.1029/2001GL014056, 2002

880 Colella, S., Falcini, F., Rinaldi, E., Sammartino, M., and Santoleri, R.: Mediterranean Ocean colour chlorophyll trends.
881 *PLoS ONE*, 11(6), e0155756. https://doi.org/10.1371/journal.pone.0155756, 2016

882 Cossarini G., Lazzari P., Solidoro C.: Spatiotemporal variability of alkalinity in the Mediterranean Sea, Biogeosciences,
883 12, 1647-1658, https://doi.org/10.5194/bg-12-1647-2015, 2015

884 Crise A., Allen J., Baretta J., Crispi G., Mosetti R., Solidoro C.: The Mediterranean pelagic ecosystem response to
885 physical forcing Progress in Oceanography 44 (1-3), 219-243., 1999

887 Crispi G., Mosetti R., Solidoro C., Crise A.: Nutrient cycling in Mediterranean basins: the role of the biological pump in
888 the trophic regime Ecol. Model.,138pp.101-114, 2001

890 Darmaraki, S., Somot, S., Sevault, F.et al. : Future evolution of Marine Heatwaves in the Mediterranean Sea. *Clim*
891 *Dyn* **53,** 1371–1392. https://doi.org/10.1007/s00382-019-04661-z, 2019

893 Di Biagio V., Cossarini G., Salon S., Lazzari P., Querin S., Sannino G., Solidoro C.: Temporal scales of variability in the
894 Mediterranean Sea ecosystem: Insight from a coupled model. Journal of Marine Systems.
895 https://doi.org/10.1016/j.jmarsys.2019.05.002., 2019

897 D'Ortenzio F. and D'Alcala M.R.: On the trophic regimes of the Mediterranean Sea: a satellite analysis. Biogeosciences
898 6 (2), 139-148, 2009

900 Diffenbaugh, N. S., Pal, J. S., Giorgi, F., and Gao, X..: Heat stress intensification in the Mediterranean climate change
901 hotspot. Geophys. Res. Lett. 34:GL030000. doi: 10.1029/2007GL030000, 2007

902 Dubois, C., Somot, S., Carillo, S. C. A., De´que´, M., Dell'Aquila, A. and co-authors: Future projections of the surface
903 heat and water budgets of the Mediterranean Sea in an ensemble of coupled Atmosphere-Ocean Regional Climate Models.
904 Clim. Dynam. 39(78), 18591884, 2012

905 Foujols M.-A., Lévy M., Aumont O., Madec G.: OPA 8.1 Tracer Model Reference Manual. Institut Pierre Simon Laplace,
906 pp. 39., 2000

908 Galli G., Lovato T., Solidoro C.: Marine Heat Waves Hazard 3D Maps and the Risk for Low Motility Organisms in a
909 Warming Mediterranean Sea. Frontiers in Marine Science 4:136. doi: 10.3389/fmars.2017.00136, 2017

911 Giorgi, F: Climate change hot-spots. *Geophysical research letters*, *33*(8).2006

913 Giorgi F, Lionello P: Climate Change Projections for the Mediterranean Region. *Glob Planet Change* 63:90-104. doi:
914 10.1016/jgloplacha200709005, 2008

916 Gualdi, S., Somot, S., Li, L., Artale, V., Adani, M., Bellucci, A., et al.: The CIRCE simulations: Regional climate change
917 projections with realistic representation of the mediterranean sea. *Bulletin of the American Meteorological Society, 94,*
918 65-81. doi:10.1175/BAMS-D-11-00136.1, 2013

919

920 Herrmann M., Diaz F., Estournel C., Marsaleix P., Ulses C.: Impact of atmospheric and oceanic interannual variability
921 on the Northwestern Mediterranean Sea pelagic planktonic ecosystem and associated carbon cycle, *J. Geophys. Res.*
922 *Oceans*, 118, 5792–5813, doi:10.1002/jgrc.20405., 2013

923

924 IPCC AR5 Climate Change 2014: Synthesis Report. Contribution of Working Groups I, II and III to the Fifth Assessment
925 Report of the Intergovernmental Panel on Climate Change, 2014

926 Kwiatkowski, L., Torres, O., Bopp, L., Aumont, O., Chamberlain, M., Christian, J. R., Dunne, J. P., Gehlen, M., Ilyina,
927 T., John, J. G., Lenton, A., Li, H., Lovenduski, N. S., Orr, J. C., Palmieri, J., Santana-Falcón, Y., Schwinger, J., Séférian,
928 R., Stock, C. A., Tagliabue, A., Takano, Y., Tjiputra, J., Toyama, K., Tsujino, H., Watanabe, M., Yamamoto, A., Yool,
929 A., and Ziehn, T.: Twenty-first century ocean warming, acidification, deoxygenation, and upper-ocean nutrient and
930 primary production decline from CMIP6 model projections, Biogeosciences, 17, 3439–3470, https://doi.org/10.5194/bg-
931 17-3439-2020, 2020

932

933 Lamon, L., Rizzi, J., Bonaduce, A. et al.: An ensemble of models for identifying climate change scenarios in the Gulf of
934 Gabes, Tunisia Reg Environ Change 31. https://doi.org/10.1007/s10113-013-0430-x, 2014

935

936 Lascaratos, A.: Estimation of deep and intermediate water mass formation rates in the Mediterranean Sea. Deep-Sea
937 Research II, 40, 1327–1332, 1993

938

939 Lazzari, P, Solidoro, C., Ibello, V., Salon, S., Teruzzi, A., Béranger, K., Colella, S., Crise, A.: Seasonal and inter-annual
940 variability of plankton chlorophyll and primary production in the Mediterranean Sea: a modelling approach,
941 Biogeosciences, 9, 217-233, doi:10.5194/bg-9-217-2012, 2012

942

943 Lazzari P., G Mattia, C Solidoro, S Salon, A Crise, M Zavatarelli, P Oddo, M Vichi : The impacts of climate change and
944 environmental management policies on the trophic regimes in the Mediterranean Sea: Scenario analyses Journal of
945 Marine Systems Sea, 2014

946

947 Lazzari, P, Solidoro C., Salon S., Bolzon G.,: Spatial variability of phosphate and nitrate in the Mediterranean Sea: A
948 modeling approach Deep Sea Research Pages 39-52, 2016

949

950 Lavigne, H., D'ortenzio, F., d'Alcalà, M. R., Claustre, H., Sauzede, R., and Gacic, M.: On the vertical distribution of the
951 chlorophyll a concentration in the Mediterranean Sea: a basin-scale and seasonal approach. Biogeosciences, 12(16), 5021-
952 5039, 2015

953

954 Lionello P., F. Abrantes, L. Congedi, F. Dulac, M. Gacic, D. Gomis, C. Goodess, H. Hoff, H. Kutiel, J. Luterbacher, S.
955 Planton, M. Reale, K. Schröder, M. V. Struglia, A. Toreti, M. Tsimplis, U. Ulbrich, E. Xoplaki: Introduction:
956 Mediterranean Climate: Background Information in Lionello P. (Ed.) The Climate of the Mediterranean Region. From
957 the Past to the Future, Amsterdam: Elsevier (NETHERLANDS), XXXV-lXXX, ISBN:9780124160422, 2012

958

959   Lovato, T., Vichi, M., Oddo, P.: High-resolution simulations of Mediterranean Sea physical oceanography under current
960   and scenario climate conditions: model description, assessment and scenario analysis. CMCC Research Paper,
961   RP0207.2013, 2013

962

963   Macias, D., Stips, A., and Garcia-Gorriz, E.: The relevance of deep chlorophyll maximum in the open Mediterranean Sea
964   evaluated through 3D hydrodynamic-biogeochemical coupled simulations. Ecological Modelling, 281, 26-37, 2014

965

966   Macias, D. M., Garcia-Gorriz, E., and Stips, A.: Productivity changes in the Mediterranean Sea for the twenty-first century
967   in response to changes in the regional atmospheric forcing. Frontiers in Marine Science, 2, 79, 2015.

968

969   Macias D., Garcia-Gorriz E., Stips A.: Deep winter convection and phytoplankton dynamics in the NW Mediterranean
970   Sea under present climate and future (horizon 2030) scenarios. Sci. Rep. 22, 1–15. https://doi.org/10.1038/s41598-018-
971   24965-0.2018, 2018

972

973   Madec, G. : NEMO Ocean Engine. Note du Pôle de modélisation, No 27, Institut Pierre-Simon Laplace (IPSL), France,
974   2008

975

976   Mantziafou A. and Lascaratos A: An eddy resolving numerical study of the general circulation and deep-water formation
977   in the Adriatic Sea, Deep Sea Res., Part I, 51(7), 251–292., 2004

978

979   Mantziafou A. and Lascaratos A.: Deep-water formation in the Adriatic Sea:Interannual simulations for the years 1979-
980   1999, Deep Sea Res., Part I, 55, 1403–1427, 2008

981

982   MedECC Climate and Environmental Change in the Mediterranean Basin: Current Situation and Risks for the Future.
983   First Mediterranean Assessment Report [Cramer, W., Guiot, J., Marini, K. (eds.)] Union for the Mediterranean, Plan Bleu,
984   UNEP/MAP, Marseille, France, 600pp, 2020

985

986   Myers PG and Haines K: Stability of the Mediterranean's thermohaline circulation under modified surface evaporative
987   fluxes. J Geophys Res 107(C3):7-1-10, 2002

988

989   Morel, A. and Gentili, B.: The dissolved yellow substance and the shades of blue in the Mediterranean Sea,
990   Biogeosciences, 6, 2625–2636, https://doi.org/10.5194/bg-6-2625-2009, 2009

991

992   Moullec, F., Barrier, N., Drira, S., Guilhaumon, F., Marsaleix, P., Somot, S., ... and Shin, Y. J.: An end-to-end model
993   reveals losers and winners in a warming Mediterranean Sea. *Frontiers in Marine Science*, *6*, 345. 2019

994

995   Moutin T. and Raimbault P.: Primary production, carbon export and nutrients availability in western and eastern
996   Mediterranean Sea in early summer 1996 (MINOS cruise), J. Marine Syst.,33/34, 273–288, 2002

997

998   Moss, R. H., Edmonds, J. A., Hibbard, K. A., Manning, M. R., Rose, S. K., Van Vuuren, D. P., Meehl, G. A.: The next
999   generation of scenarios for climate change research and assessment. Nature, 463(7282), 747-756, 2010

1000   Nittis K. and Lascaratos A.: Diagnostic and prognostic numerical studies of LIW formation. Journal of Marine Systems,
1001   18, 179–195, 1998

1002

1003   O'Connor, M. I., Gilbert, B., and Brown, C. J.: Theoretical predictions for how temperature affects the dynamics of
1004   interacting herbivores and plants. The American Naturalist, 178(5), 626-638, 2011

1005

1006   O'Neill, B. C., Tebaldi, C., Vuuren, D. P. V., Eyring, V., Friedlingstein, P., Hurtt, G., ... and Sanderson, B. M.: The
1007   scenario model intercomparison project (ScenarioMIP) for CMIP6. Geoscientific Model Development, 9(9), 3461-3482.
1008   2016

1009

1010   Oddo, P., Adani, M., Pinardi, N., Fratianni, C., Tonani, M., and Pettenuzzo, D.: A nested Atlantic-Mediterranean Sea
1011   general circulation model for operational forecasting. Ocean Science, 5, 461–473. https://doi.org/10.5194/os-5-461-2009,
1012   2009

1013   Pagès R., Baklouti, M., Barrier, N., Ayache, M., Sevault, F., Somot, S., and Moutin, T..: Projected Effects of Climate-
1014   Induced Changes in Hydrodynamics on the Biogeochemistry of the Mediterranean Sea Under the RCP 8.5 Regional
1015   Climate Scenario. Frontiers in Marine Science, 7, 957, 2020

1016

1017   Planton, S., P. Lionello, V. Artale, R. Aznar, A. Carrillo, J. Colin, L. Congedi, C. Dubois, A. Elizalde, S. Gualdi, E.
1018   Hertig, J. Jacobeit, G. Jordà, L. Li, A. Mariotti, C. Piani, P. Ruti, E. Sanchez-Gomez, G. Sannino, F. Sevault, S. Somot,
1019   M. Tsimplis: The Climate of the Mediterranean Region in Future Climate in Lionello P. (Ed.) The Climate of the
1020   Mediterranean Region. From the Past to the Future , Amsterdam: Elsevier (NETHERLANDS), Projections 449-502, 2012

1021

1022   Powley, H. R., Krom, M. D., and Van Cappellen, P. : Circulation and oxygen cycling in the Mediterranean Sea: Sensitivity
1023   to future climate change, *J. Geophys. Res. Oceans*, 121, 8230– 8247, doi:10.1002/2016JC012224, 2016

1024

1025   Reale M., Giorgi F., Solidoro C., Di Biagio V., Di Sante F., Mariotti L., Farneti R., Sannino G.: The Regional Earth
1026   System Model RegCM-ES: Evaluation of the Mediterranean climate and marine biogeochemistry. *Journal of Advances
1027   in Modeling Earth Systems*, 12, e2019MS001812. https://doi.org/10.1029/2019MS001812, 2020a

1028

1029   Reale M., Salon S., Somot S., Solidoro C., Giorgi F., Cossarini G., Lazzari P., Crise A., Sevault F.: Influence of large-
1030   scale atmospheric circulation patterns on nutrients dynamics in the Mediterranean Sea in the extended winter season
1031   (October-March) 1961-1999 *Climate Research* https://doi.org/10.3354/cr01620, 2020b

1032

1033   Richon C., Dutay J.-C., Dulac F., Wang R., Balkanski, Y.: Modeling the biogeochemical impact of atmospheric phosphate
1034   deposition from desert dust and combustion sources to the Mediterranean Sea, Biogeosciences, 15, 2499–2524,
1035   https://doi.org/10.5194/bg-15-2499-2018, 2018

1036

Richon C., Dutay J.-C., Bopp L., Le Vu B., Orr J. C., Somot S., Dulac, F.: Biogeochemical response of the Mediterranean Sea to the transient SRES-A2 climate change scenario, Biogeosciences, 16, 135-165, https://doi.org/10.5194/bg-16-135-2019, 2019

Salon, S., Cossarini, G., Bolzon, G., Feudale, L., Lazzari, P., Teruzzi, A., Solidoro, C., and Crise, A.: Novel metrics based on Biogeochemical Argo data to improve the model uncertainty evaluation of the CMEMS Mediterranean marine ecosystem forecasts, Ocean Sci., 15, 997–1022, https://doi.org/10.5194/os-15-997-2019, 2019

Schroeder K, Garcìa-Lafuente J, Josey SA, Artale V, Nardelli BB, Carrillo A, Gačić M, Gasparini GP, Herrmann M, Lionello P, Ludwig W, Millot C, Özsoy E, Pisacane G, Sánchez-Garrido JC, Sannino G, Santoleri R, Somot S, Struglia M, Stanev E, Taupier-Letage I, Tsimplis MN, Vargas-Yáñez M, Zervakisì V, Zodiatis : Circulation of the Mediterranean Sea and its Variability. in P Lionello (ed.), *The Climate of the Mediterranean Region: From the Past to the Future*. Elsevier Inc., pp. 187-256. https://doi.org/10.1016/B978-0-12-416042-2.00003-3, 2012

Scoccimarro E., S. Gualdi, A. Bellucci, A. Sanna, P.G. Fogli, E. Manzini, M. Vichi, P. Oddo, and A. Navarra: Effects of Tropical Cyclones on Ocean Heat Transport in a High Resolution Coupled General Circulation Model. Journal of Climate, 24, 4368-4384, 2011

Simoncelli, S., Fratianni, C., Pinardi, N., Grandi, A., Drudi, M., Oddo, P., and Dobricic, S.: Mediterranean Sea Physical Reanalysis (CMEMS MED-Physics) [Data set]. Copernicus Monitoring Environment Marine Service (CMEMS). https://doi.org/10.25423/MEDSEA_REANALYSIS_PHYS_006_004, 2019

Siokou-Frangou I., Christaki U., Mazzocchi M., Montresor M., Ribera d'Alcala M., Vaque D., Zingone A.: Plankton in the open Mediterranean sea: a review. Biogeosciences,7(5):1543-1586., 2010

Sitz, L. E., di Sante, F., Farneti, R., Fuentes-Franco, R., Coppola, E., Mariotti, L., Reale, M., Sannino, G., Barreiro, M., Nogherotto, R., Giuliani, G., Graffino, G., Solidoro, C., Cossarini, G., and Giorgi, F.: Description and evaluation of the Earth System Regional Climate Model (Reg CM-ES). Journal of Advances in Modeling Earth Systems, 9, 1863–1886. https://doi.org/10.1002/2017MS000933, 2017

Solidoro, C., Cossarini, G., Lazzari, P., Galli, G., Bolzon, G., Somot, S., Sevault, F., Salon, S.: Modelling carbon budgets in the Mediterranean Sea ecosystem under contemporary and future climate. Submitted to *Frontiers in Marine Sciences,* 2021

Somot S., Sevault F., Déqué M.: Transient climate change scenario simulation of the Mediterranean Sea for the 21st century using a high-resolution ocean circulation model. Climate Dynamics, Springer Verlag, 27 (7-8), pp.851-879. ff10.1007/s00382-006-0167-zff. ffhal-00195045f, 2006

Somot S., Houpert L., Sevault F., Testor P., Bosse A., Taupier-Letage I, Bouin M., Waldman R., Cassou C., Sanchez-Gomez E., Durrieu de Madron X., Adloff F., Nabat P., Herrmann, M.: Characterizing, modelling and understanding the climate variability of the deep water formation in the North-Western Mediterranean Sea. Climate Dynamics 51, 1179–1210. https://doi.org/10.1007/s00382-016-3295-0, 2018

Soto-Navarro, J., Jordá, G., Amores, A. et al.: Evolution of Mediterranean Sea water properties under climate change scenarios in the Med-CORDEX ensemble, *Clim Dyn* 54, 2135–2165. https://doi.org/10.1007/s00382-019-05105-4, 2020

Taylor, K. E., Stouffer, R. J., and Meehl, G. A.: An Overview of CMIP5 and the Experiment Design, B. Am. Meteorol. Soc., 93, 485–498, https://doi.org/10.1175/BAMS-D-11-00094.1, 2012.

Teruzzi A., Dobricic S., Solidoro C., Cossarini G.: A 3D variational assimilation scheme in coupled transport biogeochemical models: Forecast of Mediterranean biogeochemical properties, Journal of Geophysical Research, doi:10.1002/2013JC009277, 2014

Teruzzi A., Bolzon G., Salon S., Lazzari P., Solidoro C., Cossarini G.: Assimilation of coastal and open sea biogeochemical data to improve phytoplankton simulation in the Mediterranean Sea. Ocean Modelling, https://doi.org/10.1016/j.ocemod.2018.09.0072018, 2018

Teruzzi, A., Bolzon, G., Cossarini, G., Lazzari, P., Salon, S., Crise, A., and Solidoro, C.: Mediterranean Sea Biogeochemical Reanalysis (CMEMS MED-Biogeochemistry) [Data set]. Copernicus Monitoring Environment Marine Service (CMEMS). https://doi.org/10.25423/MEDSEA_REANALYSIS_BIO_006_008, 2019

Teruzzi, A., Di Biagio, V., Feudale, L., Bolzon, G., Lazzari, P., Salon, S., Di Biagio, V., Coidessa, G., and Cossarini, G.: Mediterranean Sea Biogeochemical Reanalysis (CMEMS MED-Biogeochemistry, MedBFM3 system) (Version 1) [Data set]. Copernicus Monitoring Environment Marine Service (CMEMS). https://doi.org/10.25423/CMCC/MEDSEA_MULTIYEAR_BGC_006_008_MEDBFM3, 2021

Thingstad, T. Frede, et al.: Nature of phosphorus limitation in the ultraoligotrophic eastern Mediterranean. *Science* 309.5737: 1068-1071, 2005

Van Apeldoorn, D. and Bouwman, L.: SES land-based runoff and nutrient load data (1980-2000), Deliverable 4.6, http://www.perseus-net.eu/assets/media/PDF/deliverables/3321.6_Final.pdf, last access 05-02-2020, 2014

Vichi, M., Allen, J. I., Masina, S., and Hardman-Mountford, N. J.: The emergence of ocean biogeochemical provinces: A quantitative assessment and a diagnostic for model evaluation, *Global Biogeochem. Cycles*, 25, GB2005, doi:10.1029/2010GB003867, 2011

Vichi, M., Cossarini, G., Gutierrez Mlot E., Lazzari P., Lovato T., Mattia G., Masina S., McKiver W., Pinardi N., Solidoro C., Zavatarelli M.,The Biogeochemical Flux Model (BFM): Equation Description and User Manual. BFM version 5

1115 (BFM-V5). Release 1.0, BFM Report series N, 1. March 2013. CMCC, Bologna, Italy, http://bfm-community.eu, p. 87,
1116 2015

1117

1118 Waldman, R., Brüggemann, N., Bosse, A., Spall, M., Somot, S., and Sevault, F.: Overturning the Mediterranean
1119 thermohaline circulation. *Geophysical Research Letters*, 45, 8407– 8415. https://doi.org/10.1029/2018GL078502,2018

1120

1121 Wolf-Gladrow, D. A., Zeebe, R. E., Klaas, C., Körtzinger, A., and Dickson, A. G: Total alkalinity, the explicit
1122 conservative expression and its application to biogeochemical processes. Marine Chemistry, 106(1), 287-300, 2007

1123

1124 Zunino, S., Canu, D. M., Bandelj, V., and Solidoro, C.: Effects of ocean acidification on benthic organisms in the
1125 Mediterranean Sea under realistic climatic scenarios: a meta-analysis. *Regional Studies in Marine Science*, 10, 86-96.,
1126 2017

1127

1128 Zunino, S., Canu, D. M., Zupo, V., and Solidoro, C.: Direct and indirect impacts of marine acidification on the ecosystem
1129 services provided by coralligenous reefs and seagrass systems. *Global Ecology and Conservation*, 18, e00625, 2019

1130

1131 Zunino, S., Libralato, S., Melaku Canu, D., Prato G. and Solidoro C.: Impact of Ocean Acidification on Ecosystem
1132 Functioning and Services in Habitat-Forming Species and Marine Ecosystems. *Ecosystems*
1133 https://doi.org/10.1007/s10021-021-00601-3, 2021

1134